AGU PUBLICATIONS

JGR

Journal of Geophysical Research: Earth Surface

RESEARCH ARTICLE
10.1002/2016JF004101

Key Points:
- A landscape evolution model is used to show how topographic history is influenced by regional geology
- Exhumation of different lithologies modulates the transient response to base level changes over millions of years
- Significantly different erosion and topographic histories result depending on the stratigraphic architecture, even over a small range in erodibility

Supporting Information:
- Supporting Information S1

Correspondence to:
B. J. Yanites,
byanites@indiana.edu

Citation:
Yanites, B. J., Becker, J. K., Madritsch, H., Schnellmann, M., & Ehlers, T. A. (2017). Lithologic effects on landscape response to base level changes: A modeling study in the context of the eastern Jura Mountains, Switzerland. *Journal of Geophysical Research: Earth Surface, 122*, 2196–2222. https://doi.org/10.1002/2016JF004101

Received 9 OCT 2016
Accepted 12 OCT 2017
Accepted article online 19 OCT 2017
Published online 14 NOV 2017

Lithologic Effects on Landscape Response to Base Level Changes: A Modeling Study in the Context of the Eastern Jura Mountains, Switzerland

Brian J. Yanites[1,2,3], Jens K. Becker[4], Herfried Madritsch[4], Michael Schnellmann[4], and Todd A. Ehlers[3]

[1]Department of Earth and Atmospheric Sciences, Indiana University, Bloomington, IN, USA, [2]Department of Earth and Environmental Sciences, University of Michigan, Ann Arbor, MI, USA, [3]Department of Geosciences, Universität Tübingen, Tübingen, Germany, [4]Nagra, Wettingen, Switzerland

Abstract Landscape evolution is a product of the forces that drive geomorphic processes (e.g., tectonics and climate) and the resistance to those processes. The underlying lithology and structural setting in many landscapes set the resistance to erosion. This study uses a modified version of the Channel-Hillslope Integrated Landscape Development (CHILD) landscape evolution model to determine the effect of a spatially and temporally changing erodibility in a terrain with a complex base level history. Specifically, our focus is to quantify how the effects of variable lithology influence transient base level signals. We set up a series of numerical landscape evolution models with increasing levels of complexity based on the lithologic variability and base level history of the Jura Mountains of northern Switzerland. The models are consistent with lithology (and therewith erodibility) playing an important role in the transient evolution of the landscape. The results show that the erosion rate history at a location depends on the rock uplift and base level history, the range of erodibilities of the different lithologies, and the history of the surface geology downstream from the analyzed location. Near the model boundary, the history of erosion is dominated by the base level history. The transient wave of incision, however, is quite variable in the different model runs and depends on the geometric structure of lithology used. It is thus important to constrain the spatiotemporal erodibility patterns downstream of any given point of interest to understand the evolution of a landscape subject to variable base level in a quantitative framework.

1. Introduction

Quantifying landscape evolution is important for unraveling climate-tectonic interactions, predicting sediment fluxes, and understanding geomorphic responses to climate change (e.g., Herman et al., 2013; Lease & Ehlers, 2013; Tucker & Slingerland, 1997; Whipple & Meade, 2006; Willenbring & von Blanckenburg, 2010; Willett, 1999; Yanites & Kesler, 2015). Landscapes evolve as a result of drivers (e.g., tectonics and climate) that provide the energy for geomorphic work and the resistance of the Earth's surface to that work. Lithology, a major factor in resisting erosion (Sklar & Dietrich, 2001), is spatially variable on many scales across the Earth's surface (Stock & Montgomery, 1999). Yet we still lack a robust, quantitative understanding of how the erodibility of different rock types influences landscape dynamics and modulates topographic response to external forcing.

Early geomorphic studies recognized the importance of rock type on landscape evolution (e.g., Gilbert, 1877; Powell et al., 1875), yet for a long time, there was little advancement on understanding the magnitude of relative erodibilities of different rock types. More recently, mechanistic models, laboratory measurements, and field observations suggest that the erosional resistance of geologic materials spans many orders of magnitude (Bishop & Goldrick, 2000, 2010; Bishop et al., 1985; Brocard & van der Beek, 2006; Bursztyn et al., 2015; Jansen et al., 2010; Keen-Zebert et al., 2016; Pelletier et al., 2009; Scharf et al., 2013; Sklar & Dietrich, 2001; Stock & Montgomery, 1999; van der Beek et al., 2001; Whitbread et al., 2015). However, despite over a century of research on the resiliency of different rock types to erosion, quantifying the erodibility of different rock types and its influence on landscape evolution has remained elusive (Goudie, 2016). Approaches using numerical modeling (Forte et al., 2016; Perne et al., 2017; Roy et al., 2016; Staškovanová & Minár, 2016; Tucker & Slingerland, 1996; Van Der Beek & Braun, 1998) show that even simple geometric relationships of contacts between units of contrasting erodibility can lead to complex landscape

evolution. For example, exhumation of shallow-dipping contacts can lead to both hard and soft layers exhibiting local erosion rates above and below the tectonic rock uplift rate. This results from the complexities associated with exposing either harder or softer rocks as a river cuts through a contact. The river responds to the new erodibility by increasing (in softer rocks) or decreasing (in harder rocks) the rate of erosion, and this signal is propagated upstream through the entire watershed (Forte et al., 2016; Perne et al., 2017). Therefore, erosion can increase due to the exposure of a soft layer and this increase in erosion can propagate upstream into a harder unit.

An important question emerges from the previous work that is relevant to a number of landscapes carved into bedrock: how are signals of base level change modulated by spatial and temporal changes in rock type? To address this question, we model synthetic landscapes subject to variable base level for a range of simplified rock-type geometries. In an attempt to guide our analysis toward understanding how these effects may impact a real landscape, our model is parameterized around the eastern Jura Mountains in northern Switzerland (Figure 1), where detailed lithologic, topographic, and fluvial base level history data are available. This information is used in a numerical model designed to quantify the effects of varying lithology and erodibility on the propagation of base level changes. The base level changes include spatial variations in rock uplift and incision driven by drainage capture events (Willett et al., 2014; Yanites et al., 2013; Ziegler & Fraefel, 2009). Because of our focus on the propagation of base level changes across a large area, we simplify the tectonic and lithologic geometries compared to other modeling studies of folded regions (Champel et al., 2002; Miller & Slingerland, 2006). Our analysis will focus on quantifying variations in erosion and topography as a function of erodibility and base level changes.

The sedimentary rocks of the eastern Jura Mountains comprise a roughly 1,000 m thick sequence of Mesozoic carbonates, sandstones, and shales (Figure 2). The erodibility contrast between the different rock types provides an excellent opportunity to explore how variations in rock erodibility influence landscape evolution in a region of nonsteady base level. Given that erodibility is still a poorly quantified rock property, we conduct a range of simulations to quantify the sensitivity of the model topography to plausible variations in erodibility. Different end-member scenarios for erodibilities and stratigraphic geometry are explored. The models are parameterized to reflect the well-known Neogene geologic history of the eastern Jura Mountains in a generic way and to quantify the range of erodibilities necessary to reproduce the observed topographic dependence on rock type. Following this, we explore how both spatially and/or temporally variable rock types influence erosion rates by evolving a landscape in more geologically complicated simulations. In doing so, the impacts of spatially and temporally variable lithology on landscape evolution are quantified and compared to impacts of base level changes (both stream incision and tectonic rock uplift).

Although the model was set up in relation to an actual landscape, we note that the presented results are intended to quantify the plausible range of erosional responses to lithological variations rather than a precise topographic history of the eastern Jura Mountains for which the paleoclimate, geologic, and geomorphic history is far too complex to be represented in detail (Giamboni et al., 2004; Madritsch et al., 2010; Rabin et al., 2015; Ziegler & Fraefel, 2009). We have simplified our analysis by not considering the Miocene to present climate variability of the region. Acknowledging that paleoclimatic changes can have an important impact on landscape evolution (Jeffery et al., 2013; Lease & Ehlers, 2013), especially in regions where erosion thresholds are important (Tucker, 2004), we make this simplification to isolate as best as possible the role of lithology on the topographic and denudation history of an orogen. With the previous limitations in mind, the general principles explored here are intended to provide a baseline for future studies of landscape response to climate and tectonics across lithological boundaries.

2. Geologic and Geomorphic Setting of the Model Area

The Jura Mountains (Figures 1 and 2) are an arcuate range in the foreland of the central Alps representing a type example of a thin-skinned fold-and-thrust belt (Burkhard, 1990; Laubscher, 1972). The range formed during late Miocene to middle Pliocene times when the foreland Mesozoic to Cenozoic sedimentary sequence was detached along a basal evaporitic décollement immediately above the crystalline basement (Becker, 2000; Burkhard & Sommaruga, 1998; Jordan, 1992).

The Mesozoic sediments above the basal Jura décollements consist of sequences composed of weak shales and marls that are intercalated by sections of limestones and dolomites that are comparatively resistant to

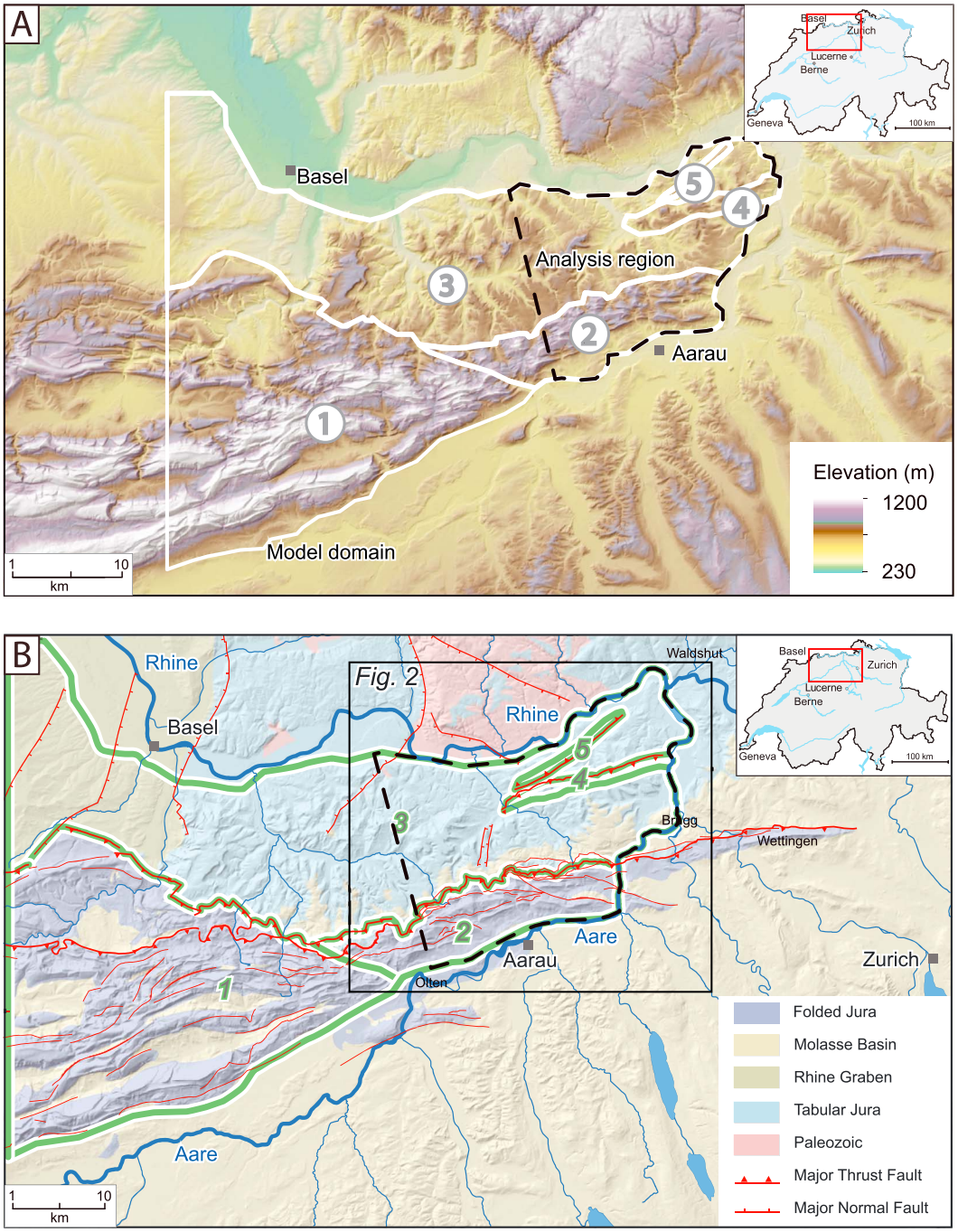

Figure 1. Topographic (a) and tectonic (b) setting of the study region encompassing the eastern Jura Mountains in northern Switzerland. White line denotes the different tectonic domains in the model setup, and black outline is the location where modern topography and model results are analyzed. The labels 1–5 in Figures 1a and 1b indicate tectonic units considered during modeling (see text for description).

erosion (Figure 1) (Diebold et al., 2005; Graf et al., 2006). The Mesozoic units are overlain by late Cenozoic clastic sediments of the external northern Alpine Molasse basin (Burkhard & Sommaruga, 1998, and references therein). The original thickness of these sediments is unknown but considered to have reached between 800 and 1,000 m at the time the Jura Mountains formed, based on apatite fission track data (Malz et al., 2015; Mazurek et al., 2006).

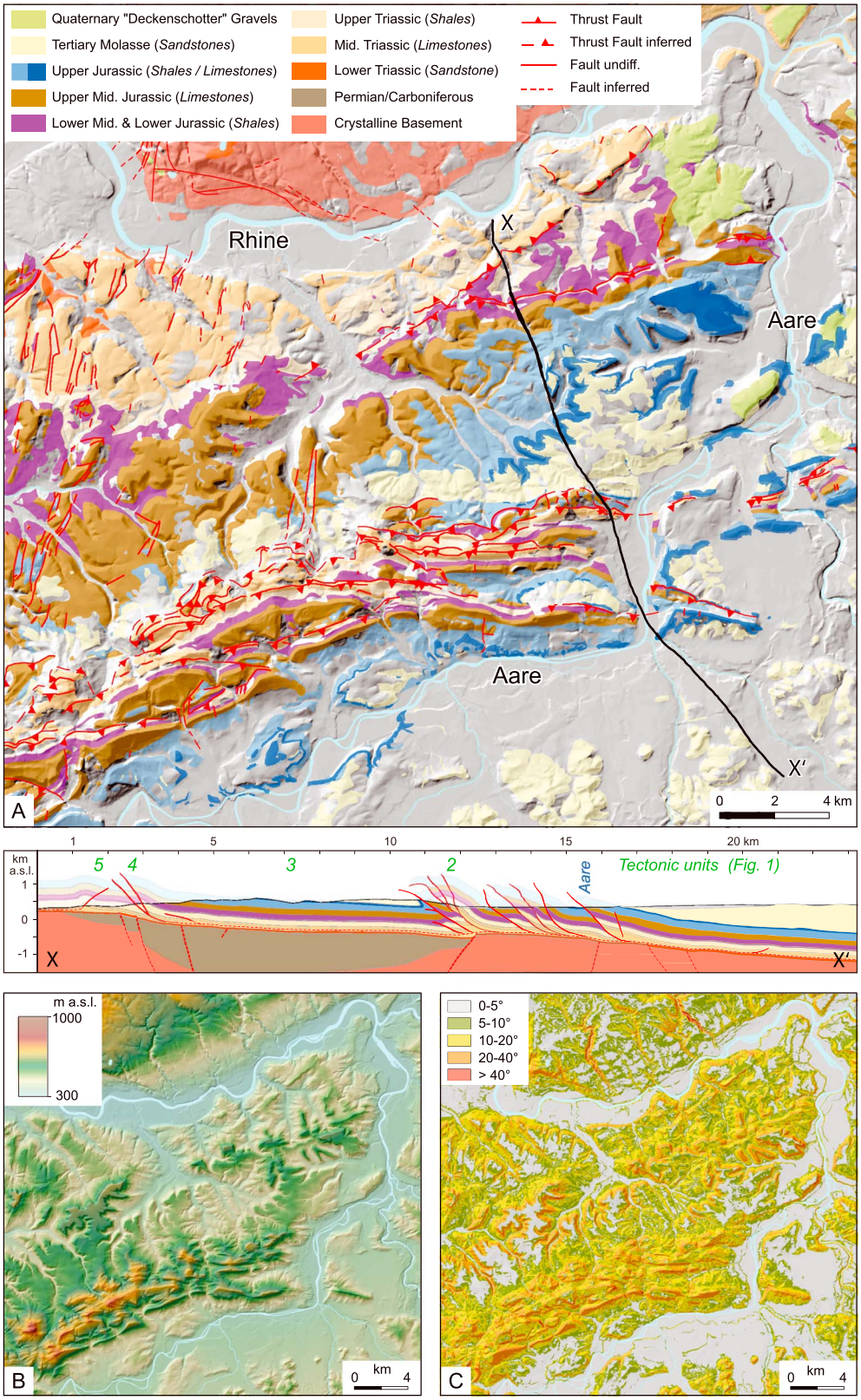

Figure 2. Geology and geomorphology of the analysis area. (a) Simplified geological map with cross section (Isler et al., 1984; Jordan et al., 2015) through the eastern Jura Mountains. Lithology classes assigned to the different stratigraphic units are given in parentheses. (b) Digital elevation model from the Swiss Federal Office of Topography (Swisstopo). (c) Hillslope gradient calculated from the DEM in Figure 2b.

The main deformation zone of the Jura fold-and-thrust belt (Folded Jura in Figure 1) is characterized by a narrow zone of higher relief compared to the surrounding landscape. The region is composed of closely spaced thrust sheets and related folds (Diebold & Noack, 1997; Malz et al., 2015) reaching approximately 500 m above the local base level formed by the Rhine River to the north and Aare River to the south and east (compare Figures 1 and 2). Weak evaporites and marls are exposed at these thrusts with more competent limestones dipping moderately to the south (Diebold et al., 2005; Graf et al., 2006). By contrast, the sedimentary succession north of the Folded Jura is almost flat lying and only thrusted locally (Figure 2). Late Pliocene to recent erosion of the units with variable erodibility has led to the development of a cuesta-like landscape rising about 200 m above the local base level (referred to as the Tabular Jura in Figure 1). The northernmost thrusts of the Jura Mountains reaching into the Tabular Jura are associated with local topographic highs rising approximately 100 m above the plateau and surface exposure of steeper dipping shales and limestones.

The main deformation phase of the Jura Mountains is considered to be a short-lived event that initiated in late Miocene times (~10 Ma) and only lasted until the early Pliocene (~3 Ma) (Becker, 2000; Madritsch, 2015; Ziegler & Fraefel, 2009). The youngest preserved Molasse deposits date from the late Miocene (~10 Ma) (Rahn & Selbekk, 2007). The timing of the end of deposition and onset of large-scale erosion remains a matter of debate (Mazurek et al., 2006; von Hagke et al., 2012; Willett & Schlunegger, 2010), but sedimentation most probably continued beyond the onset of Jura folding.

The incision history of the Rhine and Aare Rivers (Figures 1 and 2) dictates the base level of the eastern Jura Mountains. A number of previous studies have estimated rates and timing of incision along the Aare and Rhine, utilizing a series of abandoned river terraces (Preusser et al., 2011; Schlunegger & Mosar, 2010; Ziegler & Fraefel, 2009). Notably, two incision events associated with the reorganization of the Aare-Rhine system to their modern configuration are significant enough to influence the landscape history of the eastern Jura Mountains and are considered in this study. A first major event occurred at around 4.2 Ma (the capture of the Aare-Danube River system by the proto Doubs River) and a second around 2.9 Ma (marking the capture of the Aare-Doubs system by the proto-Rhine). Previous work suggests that river elevation change on the order of 400–800 m occurred due to this reorganization (Schlunegger & Mosar, 2010; Yanites et al., 2013). Therefore, this base level drop appears to contribute a significant fraction of the regional erosion. This incision around the study area likely propagated rapidly (in less than 1 Ma) due to the drainage basin size of the Rhine and Aare Rivers (Yanites et al., 2013).

In summary, the landscape evolution of the eastern Jura Mountains was mainly driven by erosion in response to tectonic rock uplift and fluvial base level changes. The geological setting of the area is therefore well suited for using numerical models to explore how variable lithology and associated erodibility potentially influence landscape evolution in a region of complex base level history.

3. Methods

We conduct a series of simulations that progressively add levels of complexity and analyze the different landscape responses (e.g., erosion rate history and topography). We compare these results to the modern topography of the eastern Jura Mountains to help define which model scenarios, and hence parameters, best represent the natural conditions in order to provide constraints on possible and plausible histories of landscape evolution in this region.

3.1. Controls of Lithology on Modern Topography

In a first step, the modern 25 m digital elevation model (DEM) of the area (Figure 2b) was resampled to 250 m (for consistency with model resolution, see below) and analyzed to quantify topographic variations among different rock types. The complex stratigraphy of the region recognized in geological maps (Figure 2) (Isler et al., 1984) was simplified and attributed to three rock types (shale, sandstone, and limestone) to represent three erodibility classes (soft, medium, and hard). The distributions of modern hillslope gradients (Figure 2c, shown for 25 m DEM for comparison with Figure 2b) and channels are extracted for these main lithological types (see Figure 3). For comparison with model results, hillslope gradients in Figure 3 are calculated based on the steepest descent in 3 × 3 grid of the 250 m pixels of resampled DEM, which is also the numerical model resolution.

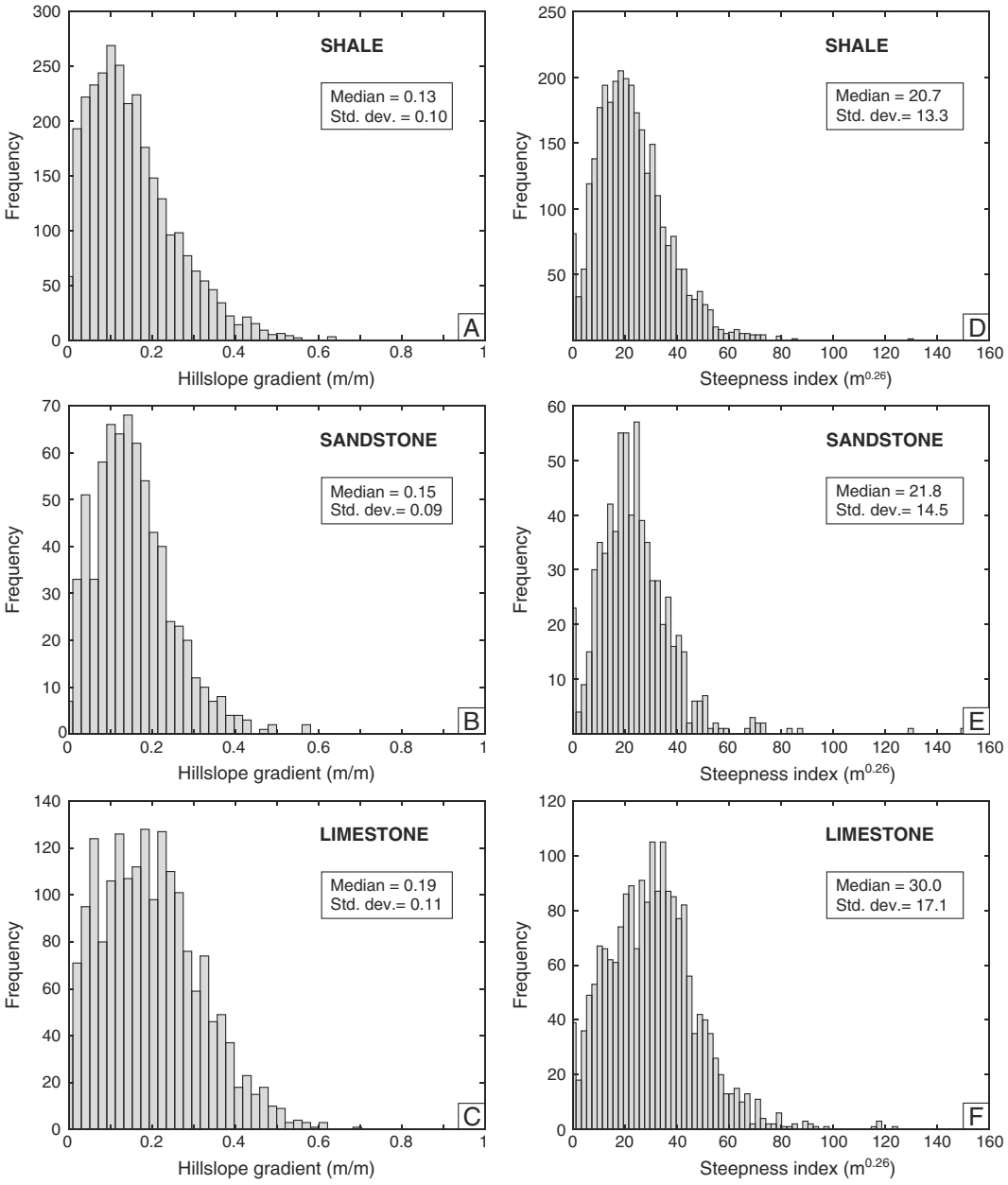

Figure 3. Distribution of (a–c) hillslope gradients and (d–f) channel steepness index, k_{sn}, for the shale, sandstone, and limestone portions of the study area topography shown in Figure 2.

Additionally, a channel steepness index, k_s (Wobus et al., 2006), is calculated using

$$k_s = \frac{A^{-\theta}}{S}. \tag{1}$$

where S is channel slope and the reference concavity (θ) and steepness (k_s) indices are calculated by regression of the log transformed values of slope and drainage area, A, across the entire river system (Wobus et al., 2006). This channel steepness index, k_s, provides a reference for how steep a local channel reach is relative to what is expected for general slope-area scaling relationships in the basin (Snyder et al., 2000). To calculate steepness, and facilitate comparison with model results, all steepness values in this study use a reference concavity of 0.44, which fits the bulk data of the study region for contributing drainage areas greater than 5×10^5 m^2. These calculations were performed over 750 m long segments of river length. Calculations on both natural and modeled landscapes used these values.

For each topographic metric, we calculate both the mean and median values of slope and steepness to compare with our model predictions. We also extract total landscape relief, which is the maximum minus the minimum elevation, and the average channel concavity across the entire landscape. These landscape metrics are used to constrain the range of erodibilities that generate similar metrics in the landscape model (see section 4.1).

3.2. Model Setup

We employ the Channel-Hillslope Integrated Landscape Development (CHILD) model (Tucker et al., 2001) to quantify the impacts of lithology and base level on geomorphic processes. To model spatially and/or temporally variable lithology, modifications were made to the software to allow the landscape to develop to a spatially variable 3-D geologic model (Figure 4). This planform landscape evolution model uses a Delaunay triangulation and Voronoi cells of irregularly spaced landscape nodes to represent the land surface (Figure 4a). The nodes store information on local properties such as elevation, rock erodibility, rock uplift, or precipitation. The depth to the next rock unit contact is tracked at each node, and the erodibility is updated when that contact is exhumed (Figure 4b).

A number of fluvial erosion models are possible in the CHILD framework. Here we focus mostly on the detachment-limited erosion model for the fluvial portion of the landscape and transport-limited diffusion model for the hillslopes (Whipple & Tucker, 2002). This is captured by the following equation:

$$\frac{\partial z}{\partial t} = U - k_f(\tau_b - \tau_d)^{P_b} - k\nabla^2 z \qquad \tau_b > \tau_d \tag{2a}$$

$$\frac{\partial z}{\partial t} = U - k\nabla^2 z \qquad \tau_b \leq \tau_d \tag{2b}$$

where z is elevation, U is the rate of rock uplift, k_f($m^{1/2}$ $s^2/kg^{3/2}$ for P_b = 1.5) is the bedrock detachment efficiency, k(m^2/yr) is hillslope erodibility for linear diffusion, τ_b is river basal shear stress, and τ_d is a critical threshold for bedrock detachment (Howard & Kerby, 1983; Tucker et al., 2001). Shear stress is calculated assuming rectangular channel shape and using Manning's equation to estimate flow depth

$$\tau_b = c_s Q^{1/3} S^{2/3}, \tag{3}$$

where c_s is a constant that includes factors such as water density and gravity and Q is water discharge (see Tucker and Slingerland, 1997, for full derivation). We vary the critical shear stress threshold in our model sensitivity analysis to explore the impact of this parameter on model results. The exponent on the excess shear stress portion of the equation, P_b, is held at 1.5 for all simulations, which results in model behavior similar to n = 1 (Whipple & Tucker, 1999) if $\tau_b \gg \tau_d$, where n is the slope exponent in the typical stream power erosion model. Hillslope diffusion is calculated between two nodes across their shared Voronoi polygon edge (the unit flux from the diffusion equation times the width of this edge, Figure 4).

This equation is solved using a finite volume approach with adaptive time stepping to ensure model stability (Tucker et al., 2001). Equations (2a) and (2b) are detachment-limited approaches to modeling river behavior and apply even in the weak Molasse sediments. We account for the Molasse by making it highly erodible, allowing for the development of the river network with a low (<50 m) overall topographic relief. However, we also test the assumption of only detachment-limited processes in a few runs by allowing transport-limited conditions when sediment loads require more energy to transport compared to the detachment of bedrock (Whipple & Tucker, 2002). When transport-limited conditions are used to model fluvial processes, the middle term in equation (2a) is represented by the divergence of sediment transport in the downstream direction:

$$\frac{\partial z}{\partial t} = U - \nabla q_f - k\nabla^2 z \qquad \tau_b > \tau_d \tag{4a}$$

$$\frac{\partial z}{\partial t} = U - k\nabla^2 z \qquad \tau_b \leq \tau_d \tag{4b}$$

where q_f is the volumetric sediment transport rate per unit width expressed as a power function of the difference between the applied, τ_b, and critical shear stress,τ_c,

$$q_f = k_t(\tau_b - \tau_c)^{3/2}, \tag{5}$$

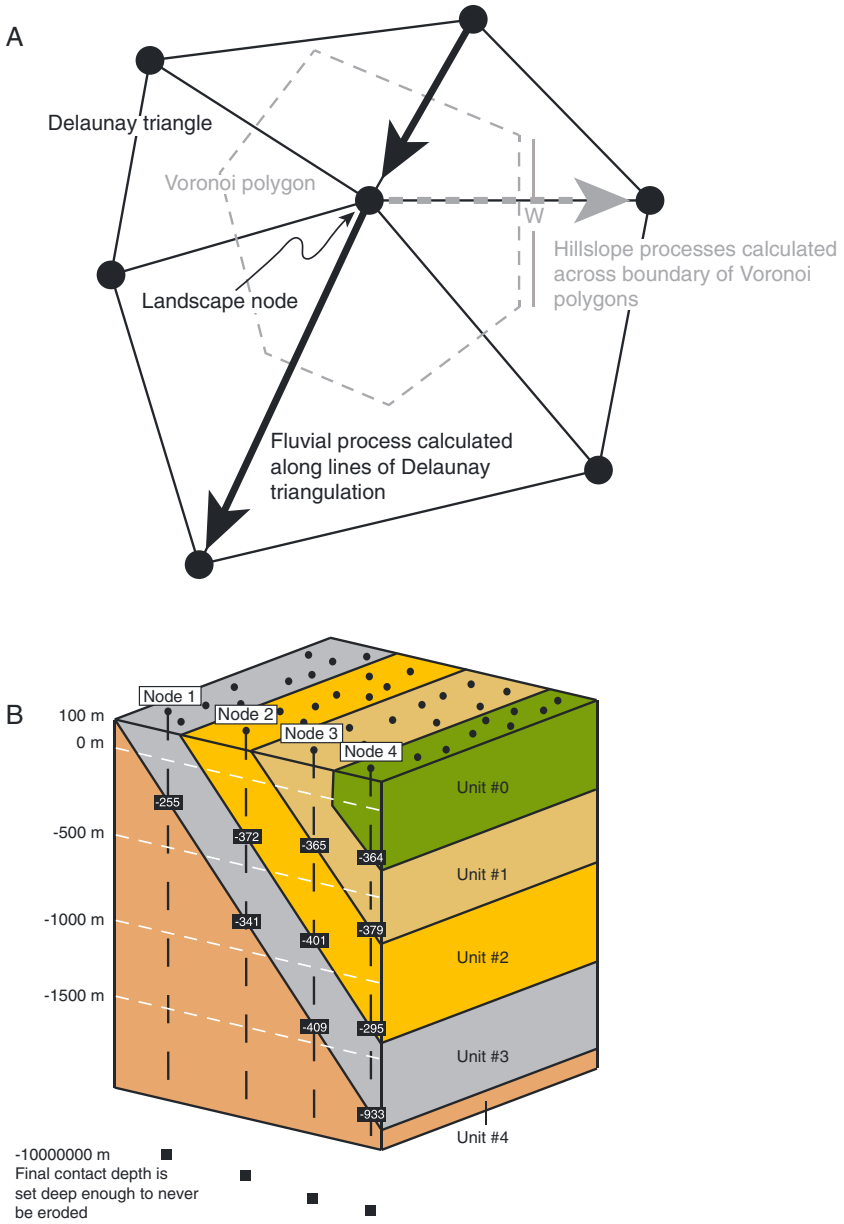

Figure 4. Schematic overview of the CHILD landscape evolution model and program modifications made to accommodate variable lithologies. (a) How the surface is constructed using Delaunay triangulations and Voronoi cells. Fluvial erosion is calculated along the steepest triangulation boundary of a node. Hillslope processes are calculated across a Voronoi cell from node to node. (b) How the program modifications allow for the representation of a 3-D geologic model where the black boxes show depth between contacts. The depth to each contact beneath the original model surface is set for each node. Total erosion since model initiation dictates which rock unit comprises the surface.

where k_t($m^{1/2}$ s^2/$kg^{3/2}$) is an empirical transport coefficient. In this case, this "mixed-channel" approach allows either detachment-limited or transport-limited behavior depending on relative roles of sediment supply and detachment rate (Whipple & Tucker, 2002). When transport-limited conditions apply, bedrock strength does not influence river processes directly, though it does influence where the transition from detachment to transport limited conditions occur in the landscape.

3.2.1. Initial and Boundary Conditions

The numerical landscape model was set up in rough relation to the geologic and geomorphic history of the eastern Jura Mountains. Modeling is focused on the area to the west-southwest of the confluence between the Aare and Rhine (Figure 1). The modern locations of the Aare and Rhine are used as model boundaries on

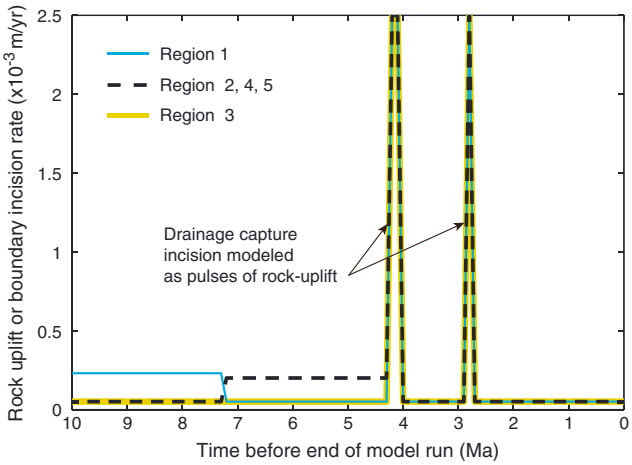

Figure 5. Timeline of site-specific rock uplift scenarios. Each line represents the rock uplift history for the five tectonic regions depicted in Figure 1. All regions are 'uplifted' during the capture events to simulate rapid incision (base level change) along the Rhine and Aare Rivers.

the north, south, and east sides of the model domain. The incision history of these rivers, and as such the base level evolution of the analysis region, is well constrained from previous modeling and data compilation studies (e.g., Yanites et al., 2013) (see discussion below). To the west of the model area, there is no proximal base level control such as a river. Therefore, the model domain is extended far enough away from the region of interest to avoid this boundary influencing drainage patterns in the analysis region (Figure 1). Note that the model results presented here are only from the analysis region marked in Figure 1 and shown in Figure 2.

The initial topographic condition used in the model includes a drainage pattern similar to the modern channel network. To accomplish this, the modern drainage pattern was etched into our initial model domain by linearly scaling the modern topography from the resampled DEM to a maximum relief of 5 m (i.e., multiplying all elevations by the quotient of 5 divided by the maximum elevation). Etching the topography in this way sets the initial drainage pattern in a relatively flat landscape and facilitates a more direct comparison between model output and modern topography. As we are primarily interested in the fluvial portion of the landscape evolution, we used a model resolution of 250 m. This has the advantage of computational efficiency allowing a broad range of assumptions on the erosion models and erodibility ranges to be explored. In the modern topography, based on the rollover in slope-area data, we infer that hillslope processes give way to channel processes between drainage areas of 0.5–1 km^2, which is only a few cells by a few cells wide (each cell is represented by a single pixel or two in the following figures). As such, we chose hillslope diffusivity and fluvial erodibility parameters that generate a similar hillslope-fluvial transition.

3.2.2. Spatial and Temporal Patterns of Base Level

Within the context of the eastern Jura Mountains, it is important to consider the spatial and temporal history of active structures and base level history (e.g., incision of the range-bounding Aare and Rhine Rivers). The tectonic setting of the eastern Jura Mountains was simplified by introducing discrete tectonic blocks in relation to the present-day structural setting (Figure 1). The tectonic blocks were discretized with varying differential rock uplift based on the reconstructed late Miocene to recent tectonics of the eastern Jura Mountains (see Becker, 2000, Madritsch, 2015, and Ziegler and Fraefel, 2009, for constraints on timing and rates).

We use the incision history of the Aare and Rhine Rivers to parameterize our model setup (Yanites et al., 2013). Previous studies showed two important quantities: (1) long-term incision along these systems is about 0.05 mm/yr and (2) pulses of incision due to river reorganization (i.e., river capture events) along the Aare and Rhine at 4.2 and 2.9 Ma produced significant base level changes (Petit et al., 1996; Schlunegger & Mosar, 2010; Yanites et al., 2013; Ziegler & Fraefel, 2009). We assume that the incision from these capture events occurred over 2×10^5 years based on the modeling work of Yanites et al. (2013), which showed that the entire profile (from capture to headwaters) adjusted over timescales of ~1 Ma.

A summary of the tectonic uplift phases and major base level modifications applied to each model simulation is shown in Figure 5. When not active, all tectonic blocks undergo background rock uplift of 0.05 mm/yr to match the long-term incision of the Rhine River. The Folded Jura west of the actual analysis area (see Region 1 outline in Figure 1 and the cross section in Figure 2) was attributed with tectonic activity between 10 and 7.2 Ma with a time averaged rock uplift rate of 0.23 mm/yr. According to local geomorphologic and structural observations (Madritsch, 2015; Ziegler & Fraefel, 2009), tectonic activity of those parts of the Folded Jura (Regions 2, 4, and 5 in Figure 1 and the cross section in Figure 2) located within the analysis area was attributed to start slightly later (between 7.2 and 4.2 Ma with an average rock uplift rate of 0.2 mm/yr). The Tabular Jura (Region 3 in Figure 1 and the cross section in Figure 2) is assumed to only have a rock uplift rate equal to the long-term background rate. The isolated thrust faults in the Tabular Jura (Regions 4 and 5 in Figure 1 and cross section in Figure 2) were also attributed with active tectonic uplift between 7.2 and 4.2 Ma at a presumed rate of 0.063 mm/yr (Madritsch, 2015; Ziegler & Fraefel, 2009). The model incorporation of folding and thrusting in the Jura Mountains as block uplifts is a simplification, and it is unclear when the tilting and folding occurred relative to the stripping of the overlying Molasse sediments (section 2). In either case,

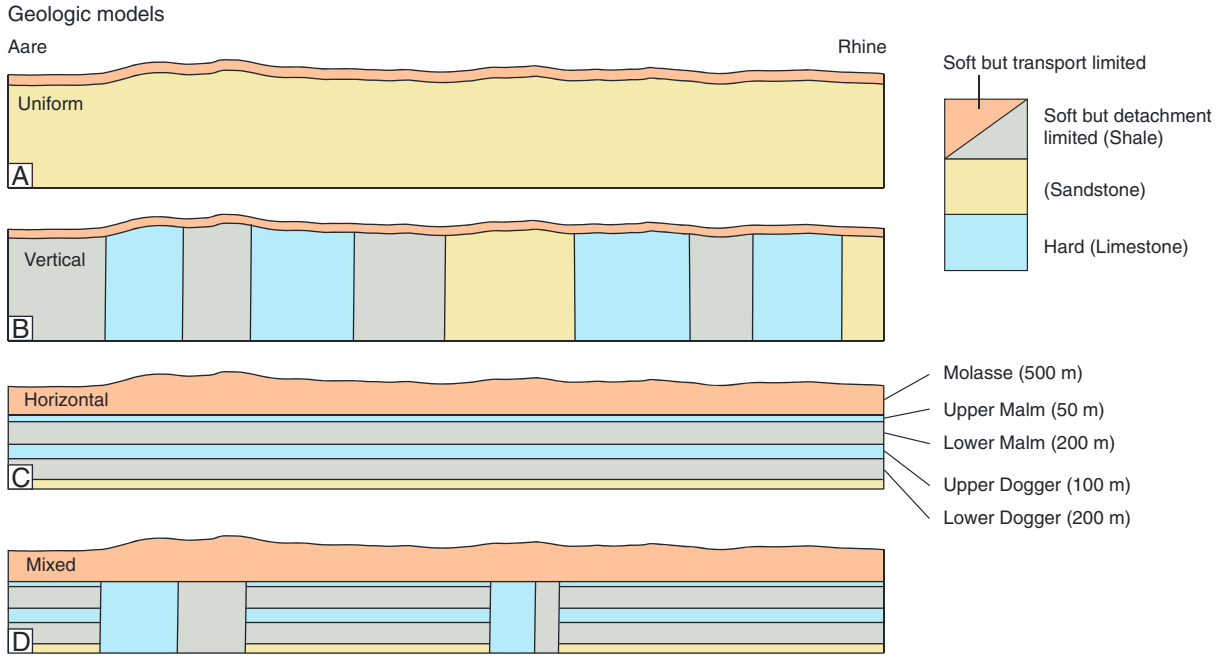

Figure 6. Schematic geologic sections of the four different lithologic scenarios considered in the landscape evolution modeling. Results for all models are shown in subsequent figures. Schematic cross sections are orientated in a north-south direction.

our focus is on the broad implications of base level signal propagation and the details of small-scale folding can be expected to have limited impact on the large-scale landscape dynamics.

In order to isolate the impacts of spatially and/or temporally variable lithology (see below), a suite of simulations was conducted using steady, uniform rock uplift (for each of the four geologic models, see Figure 6) in addition to the more specific models described above. This approach provides a baseline model for comparison to the more specific tectonic model that is described above and removes any secondary transience due to the turning on/off of individual structures or pulses of incision from drainage reorganization. This effectively isolates the impacts of heterogeneous rock type in the system. Steady uniform rates of 0.05, 0.1, and 0.2 mm/yr are simulated.

3.2.3. Lithologic Geometry

To explore the influence of complex lithologic structure on landscape evolution, we set up a series of four model simulations with increasing complexity in the geometry of rock erodibility. By sequentially adding complexity to the models, we aim to numerically explore the landscape response to spatially and/or temporally variable lithology and erodibility.

To place the results of the complex lithology models in context, we start with two simple cases (Figures 6a and 6b). These are intended to provide an expected range of erodibility values and model parameterizations by generating landscapes with similar distributions of topography as observed in the eastern Jura Mountains. In the first model geometry (Figure 6a) we assume a uniform lithology in space and time allowing a search of parameter space to identify the bulk erodibility values that reproduce the total relief (maximum elevation range) and slope patterns of the modern topography. In the second model geometry (Figure 6b) we introduce variable lithology in space (but fixed in time); hence, the lithological boundaries are vertical. This simple geometry allows the quantification of variations of erodibility required to reproduce the different observed landscape morphologies (Figure 2) but does not add the complexity of temporally changing erodibility, which occurs whenever a landscape erodes through a contact (Forte et al., 2016; Perne et al., 2017).

Using the erodibility parameters for each rock type from the second, vertical contacts simulation that best reproduced the modern topography, we explore spatial and temporal variations in erodibility applying a horizontal lithology (Figure 6c) and a mixed bedding case (Figure 6d) in rough analogy to field constraints from the eastern Jura Mountains (compare to map pattern in Figure 2).

In each of these models, a layer of poorly lithified Molasse sediments covers the top of the Mesozoic succession. The initial thickness of these sediments above the Mesozoic bedrock in the Jura Mountains prior to their formation at ~11 Ma is not precisely known in this region. To explore the implications of different initial thicknesses, simulations were conducted with different magnitudes of Molasse cover. In the model, the Molasse is easily eroded. Therefore, the Molasse must be removed in order for detachment-limited bedrock river processes that generate significant relief to occur. Our baseline simulation assumed a 10 m thickness in Molasse sediments (Figure 6), but we also explore the implications of this parameter choice and ran a simulation with an initial thickness of 800 m. The reason to test the sensitivity of a thicker Molasse sequence is that some regions may have had significant fill early on in the deformation sequence. We note that the initial Molasse deposits resting on top of the Mesozoic units prior to the formation of the Jura Mountains were wedge shaped though this is likely negligible given the very small size and location of the modeled basin area. In other words, because the study area is near the eastern edge of the Jura Mountains, the wedge-shaped lens of Molasse was likely thin. Moreover, modeling showed that variations in the thickness of Molasse deposits would not exert a significant impact on the general results due to their fast erosion at an early stage of the model.

3.2.3.1. Spatially Uniform and Temporally Steady Erodibility Simulations (Baseline Model)

We first model the landscape under uniform erodibility (Figure 6a) to establish a baseline erodibility value. These experiments also serve to quantify the sensitivity of topographic outcomes in the model domain to different assumptions about the base level history and erosional processes. An ensemble of model simulations was conducted to explore the topographic sensitivity to erodibility, erosion mechanism, tectonics, and climate (supporting information Table S1). First, erodibility values (k_f, equations (2a) and (2b)) were varied in order-of-magnitude increments over a range of 3 orders of magnitude (simulations UL001–UL003)

Next, different assumptions on the physics of erosion processes were explored (see, e.g., Whipple and Tucker, 2002, for further information). In simulations UL004–UL007, the critical threshold (τ_d) values for erosion were varied from 10 to 100 Pa. In simulations UL010–UL013, we also tested the assumption of detachment-limited erosion and allowed transport-limited erosion (equations (2a) and (2b)) to occur where the sediment load is high (Whipple & Tucker, 2002). Finally, we explored different hillslope diffusivity values (simulations UL008–UL009 and UL014–UL015) to test if the choice of this value influences the transient response of the landscape.

3.2.3.2. Spatially Variable but Temporally Steady Erodibility Simulations (Vertical Contacts)

A suite of simulations was conducted with spatially variable but temporally constant (Figure 6b) erodibility using the range of acceptable erodibilities found in the uniform lithology models as a starting point. The spatial distribution of surface geology from a 1:100,000 scale map (Isler et al., 1984) is used to distribute lithology across the model domain. As outlined earlier, we classified the units into one of three erodibility classes, which for simplicity we refer to as limestone (low erodibility), sandstone (moderate erodibility), and shale (high erodibility). Because we are interested in the long-term evolution, we ignore mapped Quaternary units and use a nearest-neighbor algorithm to classify model nodes covered with Quaternary sediments as limestone, sandstone, or shale. We take the values for different lithologies from the previous section as the mean value and then explore twofold, tenfold, and 100-fold differences in the minimum and maximum of erodibilities (simulations VL001–VL003). Next, an ensemble of simulations was conducted exploring the different physical erosion assumptions and different climate and tectonic regimes (supporting information Table S1). We also explored the implication of different hillslope diffusivity values among the different rock types. Hillslope diffusivity captures the processes that drive detached regolith down slopes and into rivers. Because the material is already detached, it is unknown how this value varies among different rock types. Nonetheless, different values are explored to see how important this parameter may be in reproducing the modern topography.

3.2.3.3. Spatially and Temporally Variable Erodibility Simulations (Horizontal Lithology)

Introducing horizontal lithology variations in the model (Figure 6c) adds to the complexity of spatial and temporal variations in erodibility. Two base level scenarios are tested (steady versus nonsteady). The first scenario is steady rock uplift with rates of 0.2, 0.1, and 0.05 mm/yr to isolate the impacts of evolving lithology. The second scenario tests the response to pulses of base level fall driven by capture events and tectonic rock uplift (see section 2). By comparing erosion rate histories at a few key locations between the steady rock uplift with the tectonic scenario, we explore the competing effects of stratified lithology and tectonic history on

landscape evolution. Finally, we reran the tectonic scenario for a range of erodibility values and other geomorphic model parameters (i.e., similar to the vertical contacts simulations) to further explore sensitivity of the model assumptions (supporting information Table S2).

3.2.3.4. Spatially and Temporally Variable Erodibility Simulations (Mixed Vertical-Horizontal Lithology)

The final geologic model considered here (Figure 6d) mimics the present-day structural setting of the analyzed region (compare Figure 2 section with Figure 6d; note that cross sections in Figure 6 are oriented north-south in map view). Blocks of vertical lithology and contacts in the model simplistically represent the steeply dipping thrust zones of the Folded Jura separate regions with flat-lying strata as found in the Tabular Jura (compare Figures 1 and 2 with cross section). We focus these nonsteady experiments on illustrating how increasing geologic complexity influences the erosion history of a region such as the eastern Jura Mountains. This model starts with 500 m of Molasse covering the entire domain. The Molasse is underlain by either vertical or horizontal units depending on the tectonic unit (Figures 1 and 2). We simulate the same base level scenarios as in the horizontal experiment (section 3.2.3.3).

3.3. Analysis of Results and Identification of Best Fit Model Results

Model results were evaluated using four topographic metrics: total landscape relief, landscape channel concavity index, channel steepness indices, and hillslope gradient. Values for channel concavity and total relief were estimated for the entire landscape. Slope-area data were regressed for basins larger than 5×10^5 m^2 to estimate concavity. However, steepness of the different rock types was calculated using the modern value of 0.44 so that the values retained the same units and were thus comparable. Channel steepness and hillslope gradient were calculated for the different rock types. The model-predicted values for these metrics were compared to observed values for the analysis region (sections 3.1 and 4.1 and Figure 3). Thus, these four parameters capture the combined hillslope and fluvial topographic responses to different erodibility configurations (Figure 7). Figure 7 illustrates the broad range of model response, among the different topographic metrics, that can occur for the range of model parameterizations considered here. Even though our focus is on fluvial parameters, we analyze hillslope metrics for two reasons: (1) transient fluvial signals propagate to the hillslopes, influencing the morphology, and (2) we conducted a few simulations with different hillslope diffusivities. Results are shown for each topographic metric predicted in individual simulations for comparison to modern topography (see section 4.1 below). Finally, each model-predicted topography is evaluated to identify simulations that reproduce eastern Jura Mountains topography to within 50% of all topographic metrics. We chose this value because it limits the good fit simulations to anywhere from one to four runs for each level of model complexity. Among these good fit simulations, we further explore the spatial patterns of topography and lithology to further consider the model results in the context of the eastern Jura Mountains. Factors such as locations and patterns of drainage divides relative to both the model domain and lithology distributions help distinguish among the model runs.

4. Results

4.1. Modern Topographic Analysis

Observed slope distributions are variable in the primary lithology groups present in the eastern Jura Mountains (Figure 3). Moreover, separating the landscape between hillslope gradient and fluvial channel steepness reveals differences among the different rock types (Figure 3). In general, hillslopes underlain by limestone have the highest hillslope gradients and channel steepness (Figures 3c and 3f), which is statistically higher (at the 95% confidence level) than sandstone and shale according to an unpaired *t* test. The sandstone/marl and the shale portions of the landscape are statistically indistinguishable (Figures 3a, 3b, 3d, and 3e). As we will show with the numerical modeling results, the differences in morphology are not directly reflective of differences in erodibility. This is because of the history of both base level and rock-type exposure causing complexities in the distributions of topography in relation to rock type due to the transient effects of temporally variable lithology (Forte et al., 2016; Perne et al., 2017).

The modern relief of 720 m in the study region (Figure 2b) provides an additional target to calibrate the model and test for sensitivity. Total landscape relief reflects the integrated effects of tectonics, lithology, and climate from river mouth to the drainage divide. Moreover, simple landscape geometry can have an impact on relief because longer rivers can generate higher relief as relief is the integral of slopes from the

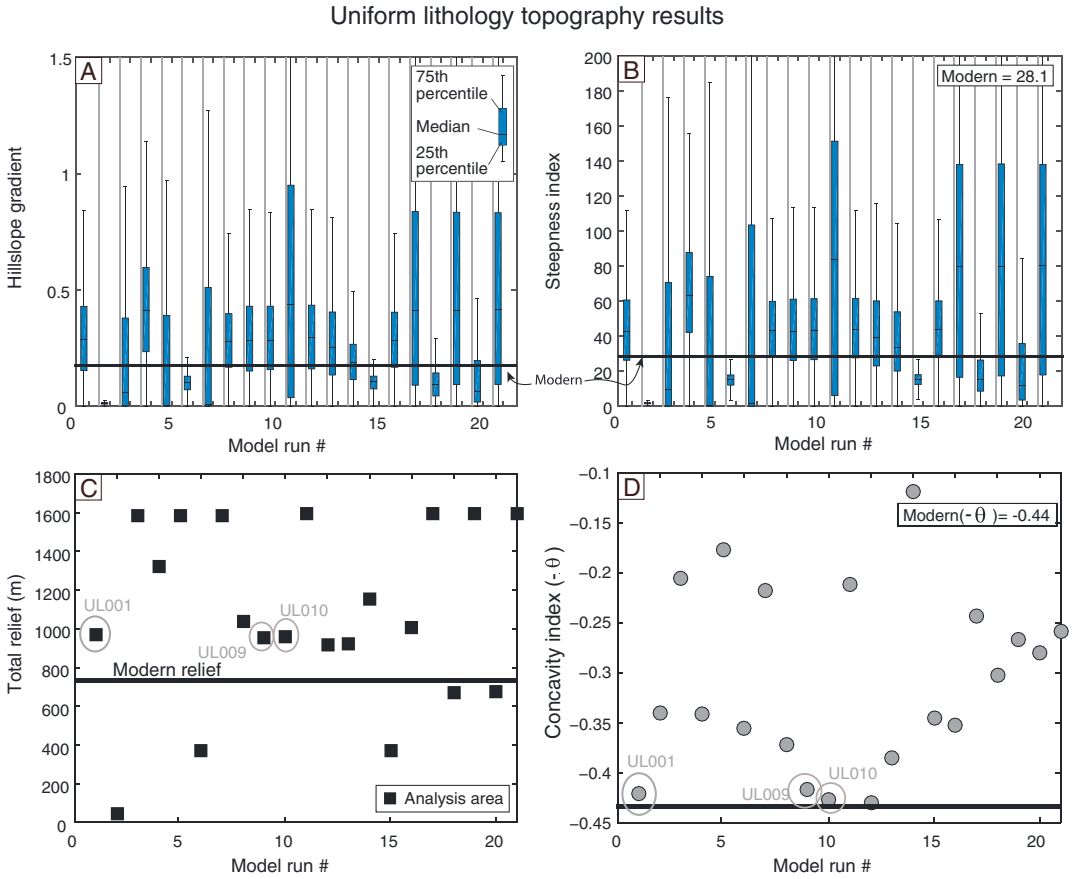

Figure 7. Topographic outcomes of the uniform lithology simulations. Model runs that consistently reproduced topography across all metrics are circled and labeled. (a) Modeled hillslope gradient distributions are illustrated with box and whisker plots that show the median (central line) and 25th and 75th percentiles (box). (b) Box and whisker plot of the channel steepness index. (c) Modeled and observed total relief. (d) Modeled and observed channel concavity index. The parameters used in each model run are provided in supporting information Tables S1 and S2.

headwaters to base level. Therefore, the total relief represents a bulk representation of network dynamics with environmental forcing.

4.2. Topographic Model Results

4.2.1. Spatially Uniform and Temporally Steady Lithology Simulations (Baseline Model)

The best fit uniform erodibility that captures the four landscape metrics using the base level history described in section 3.2.2 was found in model simulations UL001, UL009, and UL010 (Figure 7). These simulations provide bounds on erodibility values when considering only detachment-limited erosion processes. For the tectonic and climate parameter set, a bulk erodibility of 10^{-6} (m^2 s/kg) provides the best representation of topography. The uniform lithology generates topographic patterns that have monotonic trends toward the model boundary (Figure 8). For example, landscape slope increases monotonically from the model edge toward the drainage divides (Figure 8d). This is an important distinction from nonuniform model runs described below. The total relief is sensitive to erodibility, tectonics, and climate. Increasing the erodibility (simulation UL002 versus UL001) by a factor of 10 lowers landscape relief by almost a kilometer (Figure 7c). The inclusion of an erosion threshold or allowing for transport-limited behavior slightly influences total relief (e.g., simulation UL010, Figure 7), but it is not identified as a primary control on the relief of the eastern Jura Mountains. Hillslope diffusivity, as expected given the model resolution, has little impact on the overall morphology of the landscape. The only noticeable effect is "smoother" hillslopes for higher diffusivities. As the roughness/smoothness of interfluves is not a metric we are comparing model output against, changing hillslope diffusivity has little impact on which model parameter sets best describe the topography around the eastern Jura Mountains.

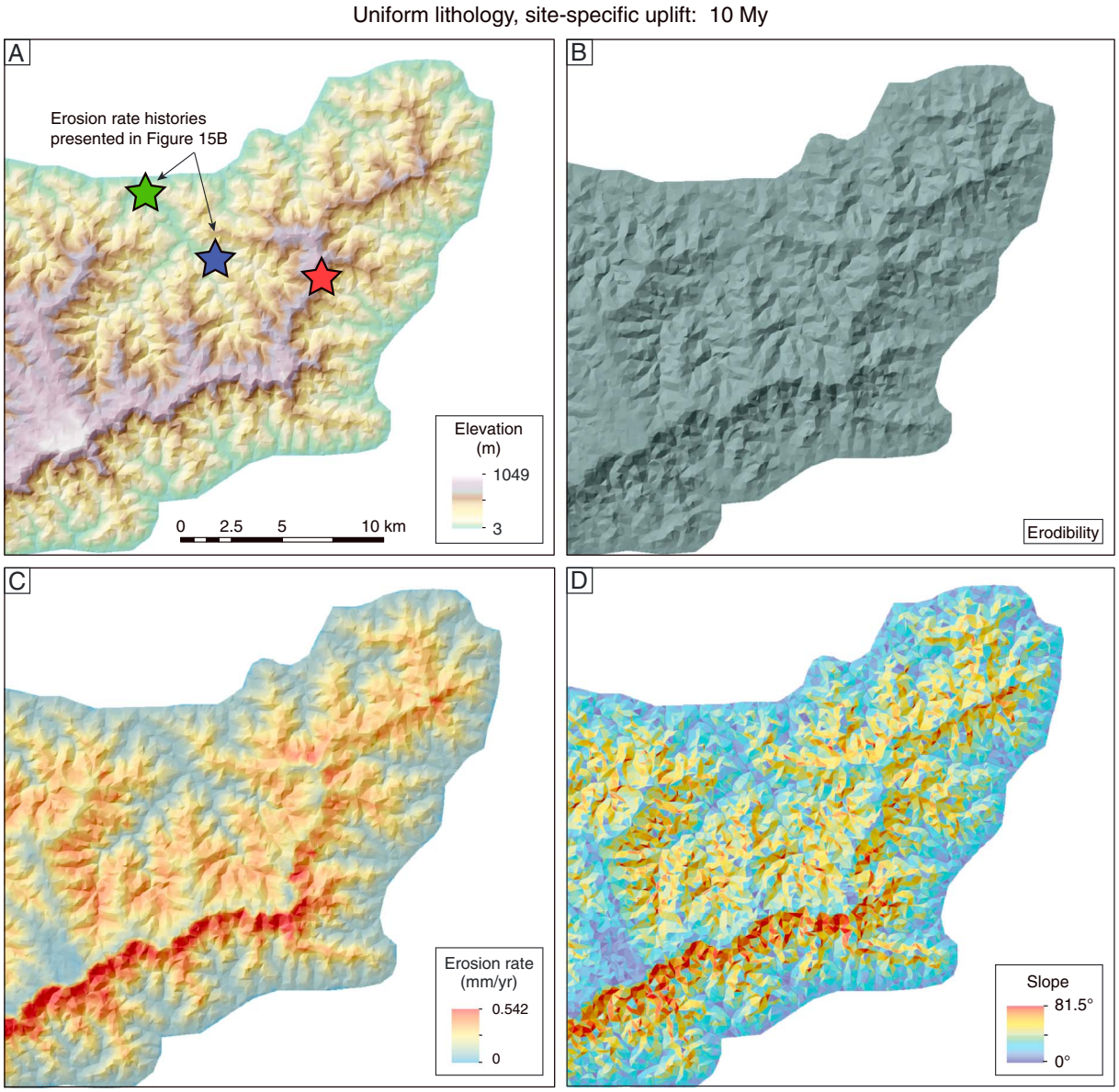

Figure 8. Topography of the best fit uniform lithology run (UL008) at 10 Ma of model run time. Rock uplift was driven by the specific spatially and temporally variable base level history of the eastern Jura Mountains as described in section 3.2.2. (a) Modeled topography and locations of erosion rate histories that are discussed later (Figure 15). (b) Erodibility map used in the simulation, which is just one rock type for these simulations. (c) The spatial distribution of modeled erosion rates in the study area and (d) the distribution of modeled landscape slopes.

4.2.2. Spatially Variable but Temporally Steady Erodibility Simulations (Vertical Contacts)

For the vertical contacts cases (variations in erodibility in space but not time), similar mean and median landscape slopes of the model output and the modern landscape are produced with a twofold difference in erodibility values that range from 1×10^{-6} for limestone to 2×10^{-6} for shale (Figure 9 and Table S1). We note, however, that the model simulation using the tectonic model (model VL019) that best reproduces modern topography has a mean erodibility among the different rock types of 1.5×10^{-6}, which is 50% higher than the erodibility of the best fit uniform lithology simulations. We find that an erodibility of limestone equal to 1×10^{-6} provides a reasonable landscape in the topography underlain by limestone. For example, mean hillslope gradients in limestone portions of the landscape in model VL019 are 0.19, which is statistically indistinguishable from the 0.21 found in the limestone portions of the modern landscape. We note, however, that the clear transience occurring in these landscapes limits the ability to directly relate topographic metrics with

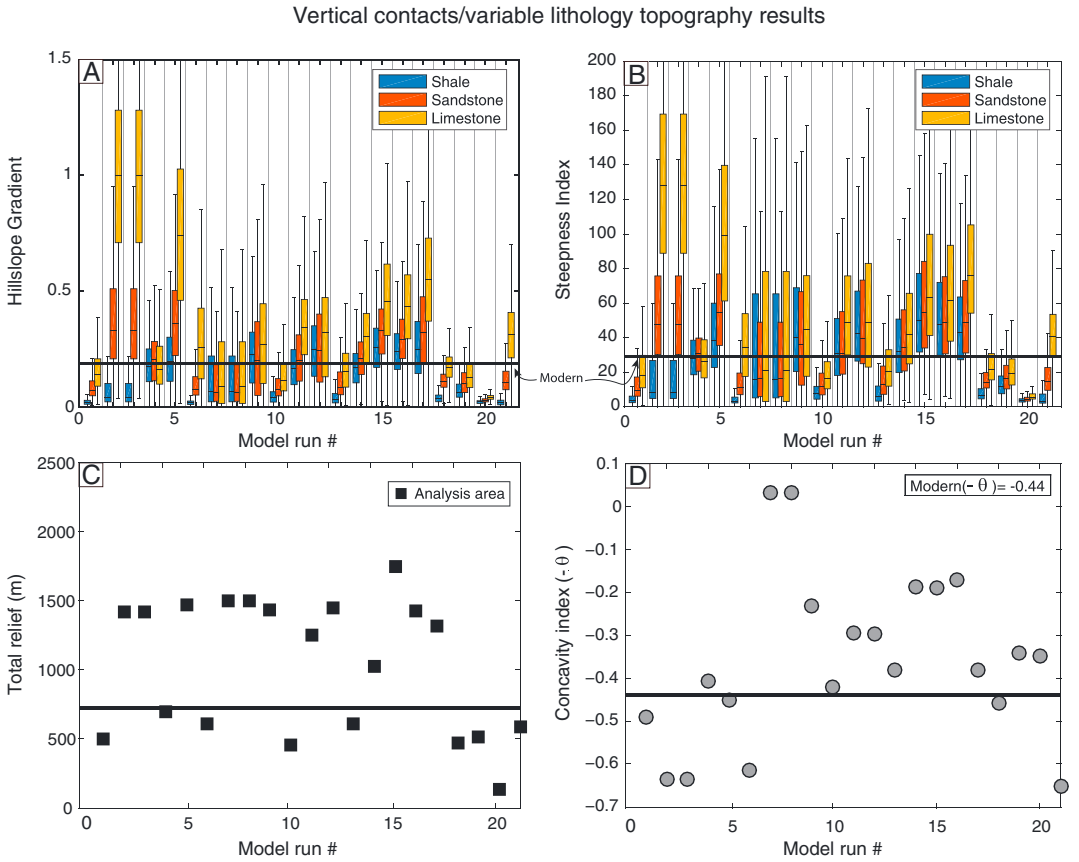

Figure 9. Topographic outcomes of the vertical lithologic contacts simulations. (a) Modeled hillslope gradient distributions are illustrated with box and whisker plots that show the median (central line) and 25th and 75th percentiles (box). Each model run number has three box and whisker plots for each lithologic type. (b) Box and whisker plot of the channel steepness index. (c) Modeled (symbols) and observed (line) total relief. (d) Modeled (symbols) and observed (line) channel concavity. The parameters used in each model run are provided in supporting information Tables S1 and S2.

lithologic resistance as hard rocks and softer rocks can be steeper at different times in a model run (Forte et al., 2016). Such complexity in landscape evolution in lithologically variable terrain makes topographic metrics a difficult approach to distinguishing between model runs. Because of this, we also perform visual quality checks on the landscape to ensure that the resulting landscapes are reasonable representations of the modern topography.

More importantly, we also find that model VL019 reproduces important patterns in topography that are not reproduced in the uniform lithology simulations (compare Figures 2, 8, and 10). For example, the drainage divide in VL019 does not decline monotonically in elevation from the southwest to the northeast. Instead, the spatial difference in erodibility causes local minima and maxima in the elevation of the drainage divide (Figure 10). This is also observed in the modern topography, where the lower elevation drainage divides are located in shale, and the limestone areas produce the steep and high drainage divides near the southern part of the study region.

Profile views of the pattern of erosion rates at different time steps also provide insight into the influence of lithology on landscape evolution (Figure 11, with traces of cross sections shown in Figure 10c). In the N-S profile (Figure 11a), we see that a portion of the landscape underlain by limestone (Figure 11c) continues to lag the rate of rock uplift (dashed line) at 5 Ma (blue line) even though the rest of the landscape is eroding at or above the rate of rock uplift. The lithologically driven reduction in rates of geomorphic processes results in a local increase in elevation as uplift outpaces erosion. The added elevation increases local topographic gradients. Following a decrease in rock uplift rates, due to the cessation of deformation on the local faults, the areas underlain by limestone erode at rates higher for a longer period than the surrounding landscape

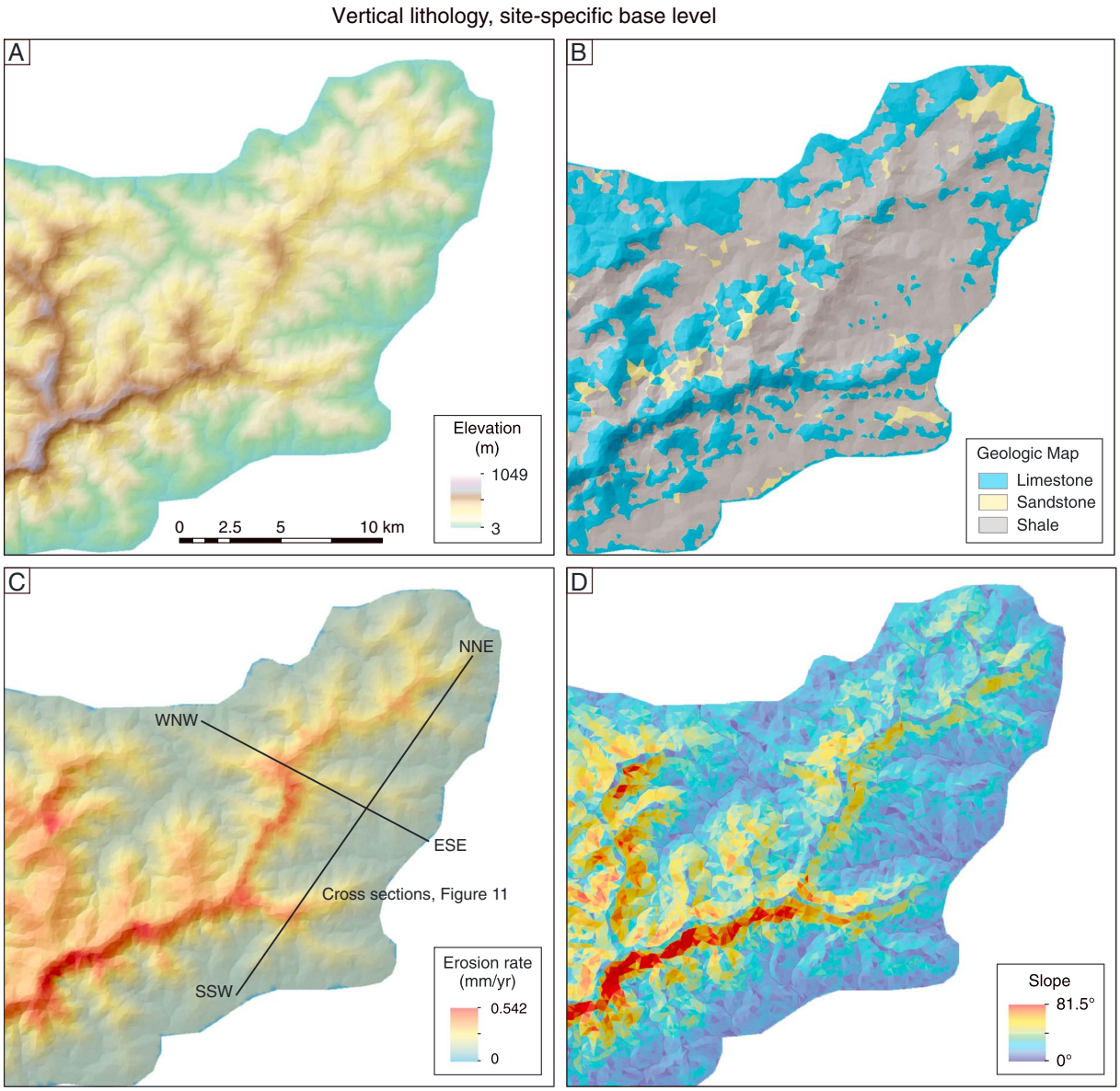

Figure 10. Topography of the best fit vertical lithologic contacts simulation (VL019) at 10 Ma. (a) Modeled topography. (b) Erodibility map used in the simulation. (c) The spatial distribution of modeled erosion rates in the study area and the location of cross sections shown in Figure 11 and (d) the distribution of modeled landscape slopes.

because of the steeper topography. The longer response timescale is because the higher (and steeper) topography created earlier in the landscape history has more mass that needs to be removed in order to lower the slopes. In other words, when high rates of uplift cease, the weaker rocks (i.e., shale) adjust their slopes to the lower base level fall rate more rapidly than the harder rocks (i.e., limestone) even though they may be initially eroding at the same rate (Whipple, 2001).

4.2.3. Spatially and Temporally Variable Erodibility (Horizontal and Mixed Lithology)

We find that model simulation HL047 (Table S2) best reproduces modern topography though key differences exist (Figure 12). For example, although average channel steepness and hillslope gradients are consistent with the modern topography, the overall relief in the analysis region is noticeably lower in the model (~470 m, Figure 12c). The best fit erodibilities are a factor of 3 greater than in the vertical contacts case (i.e., more erosive, softer material), suggesting that the layer-cake stratigraphy offers additional impedance on erosional processes. This is because of the lateral expansion of the exposure of harder layers as they are

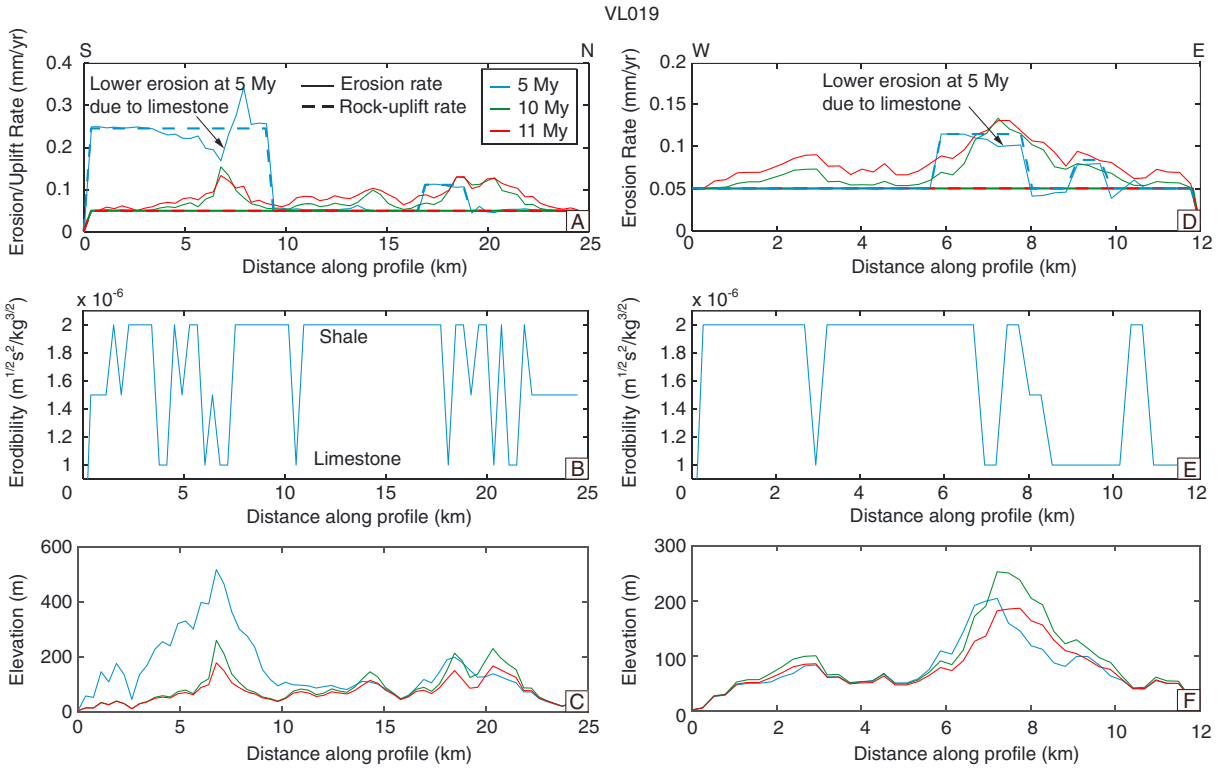

Figure 11. Cross sections at different time slices for model run VL019 (Figure 10), the best fit vertical lithologic contact case. (a) The erosion rates and uplift rates (dashed lines) at 5, 10, and 11 Ma (straight and dashed lines colored by time slice) for the south to north cross section depicted in Figure 10c. (b) The distribution of erodibility along this profile (high values are shale and low are limestone). (c) The topographic cross section at the same time slices as in Figure 11a. (d–e) The same variables as Figures 11a–11c but for the west to east cross section.

exhumed (Figure 13), whereas in the vertical contacts case, the horizontal extent of the hard layers is limited by the temporally stable contact locations (Figure 10).

We also find that the distribution of lithology is significantly different from the modern geology (compare Figures 1, 2, and 13), though this can be expected given the differences in structural geometry. Interestingly, shale makes up the bulk of the drainage divide in the model run, which is different from the modern geology for which limestone makes up the divides. This is a common result of models using horizontal lithology where shale is sandwiched between hard layers. As the underlying hard layer is exposed, it lowers the upstream rate of base level fall, creating a broad soft rock platform that undercuts the upper hard layer, leaving the divide composed of the softer layer (Forte et al., 2016; Perne et al., 2017). Because the erodibility of higher-order drainage systems near the drainage divide is central to controlling total landscape relief (Whipple & Tucker, 1999), the existence of shale at the divide in model HL047 is the reason that the model provides a poor fit on total relief yet reproduces the other topographic parameters well. In other words, the lower overall relief, but otherwise well fit topography, is a result of the softer material making up the landscape near the drainage divide where a significant portion of the topographic relief resides and is a product of the purely horizontal stratigraphy.

In the mixed vertical-horizontal lithology case, the locations of vertical bedding of limestone generate ridgelines at the vertical contact with the shale (Figure 14). The complexity of the topography and the drainage divide is quite similar to the modern topography (Figure 2).We note, however, that allowing variable lithologic bedding orientations essentially adds another degree of freedom in the modeling, and as such, a more complex topography should be expected. Even so, these similarities are quite striking, highlighting the importance of the 3-D geological representation in modeling landscapes with complex lithologic geometries (Brocard & van der Beek, 2006; Forte et al., 2016; Perne et al., 2017). Moreover, the variability in contact angles plays an important role in controlling the spatial and temporal pattern in topography in lithologically complex terrains.

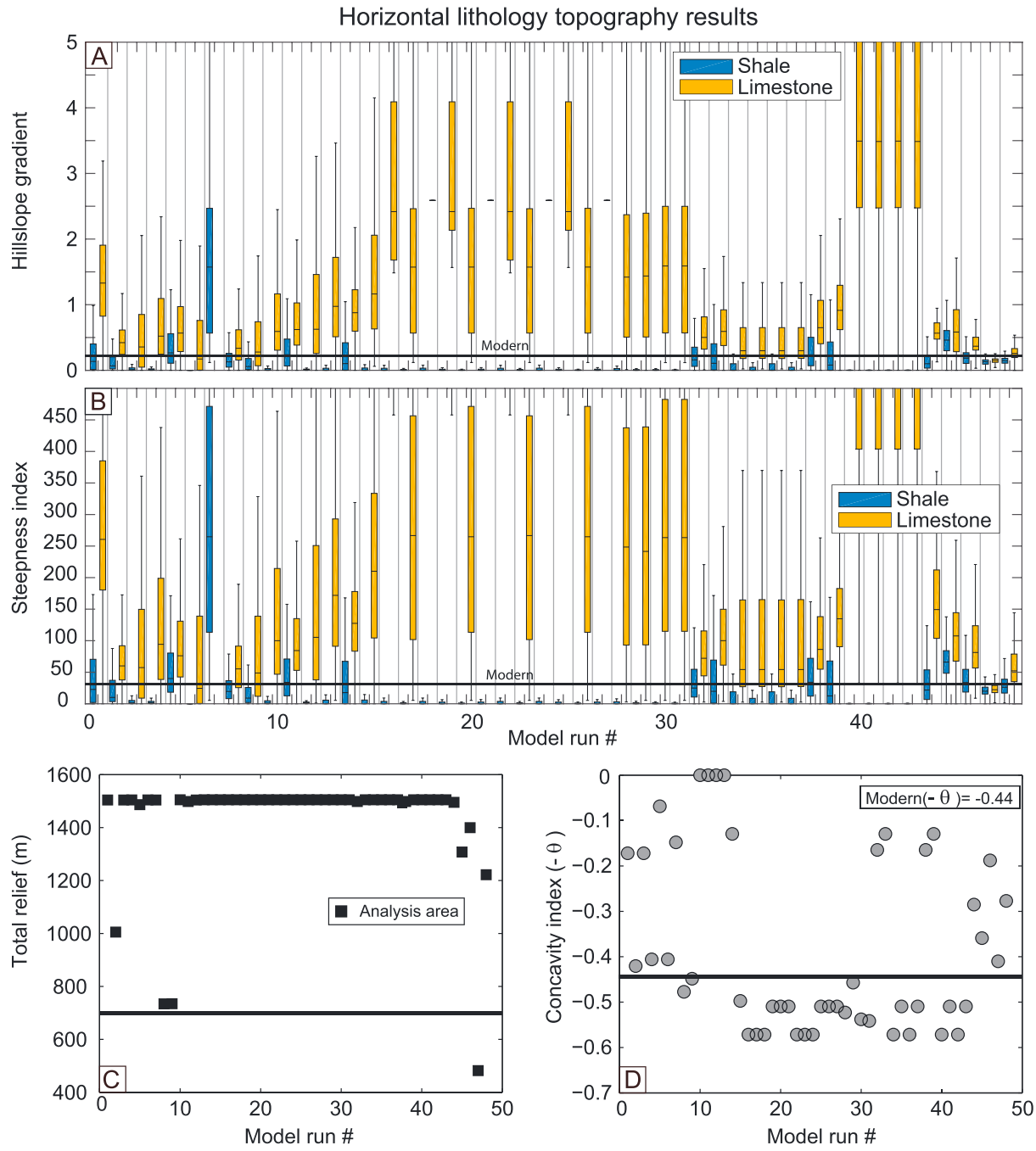

Figure 12. Topographic outcomes of the horizontal lithology (Figure 6c) runs. (a) Modeled hillslope gradient distributions are illustrated with box and whisker plots that show the median (central line) and 25th and 75th percentiles (box).Each model run number has three box and whisker plots for each lithologic type. (b) Box and whisker plot of the channel steepness index. (c) Modeled (symbols) and observed (line) total relief. (d) Modeled (symbols) and observed (line) channel concavity. The parameters used in each model run are provided in supporting information Tables S1 and S2.

4.3. Erosion Rate Histories

For each model simulation, we extract erosion rate histories at three locations (Figure 8a) along a major river to explore the spatial differences in the temporal landscape history. We extract an erosion rate history near the model edge/base level (green star Figure 8a), midriver (blue star, Figure 8a), and near the local drainage divide (red star, Figure 8a) for the results shown in Figures 8, 10, 13, and 14.

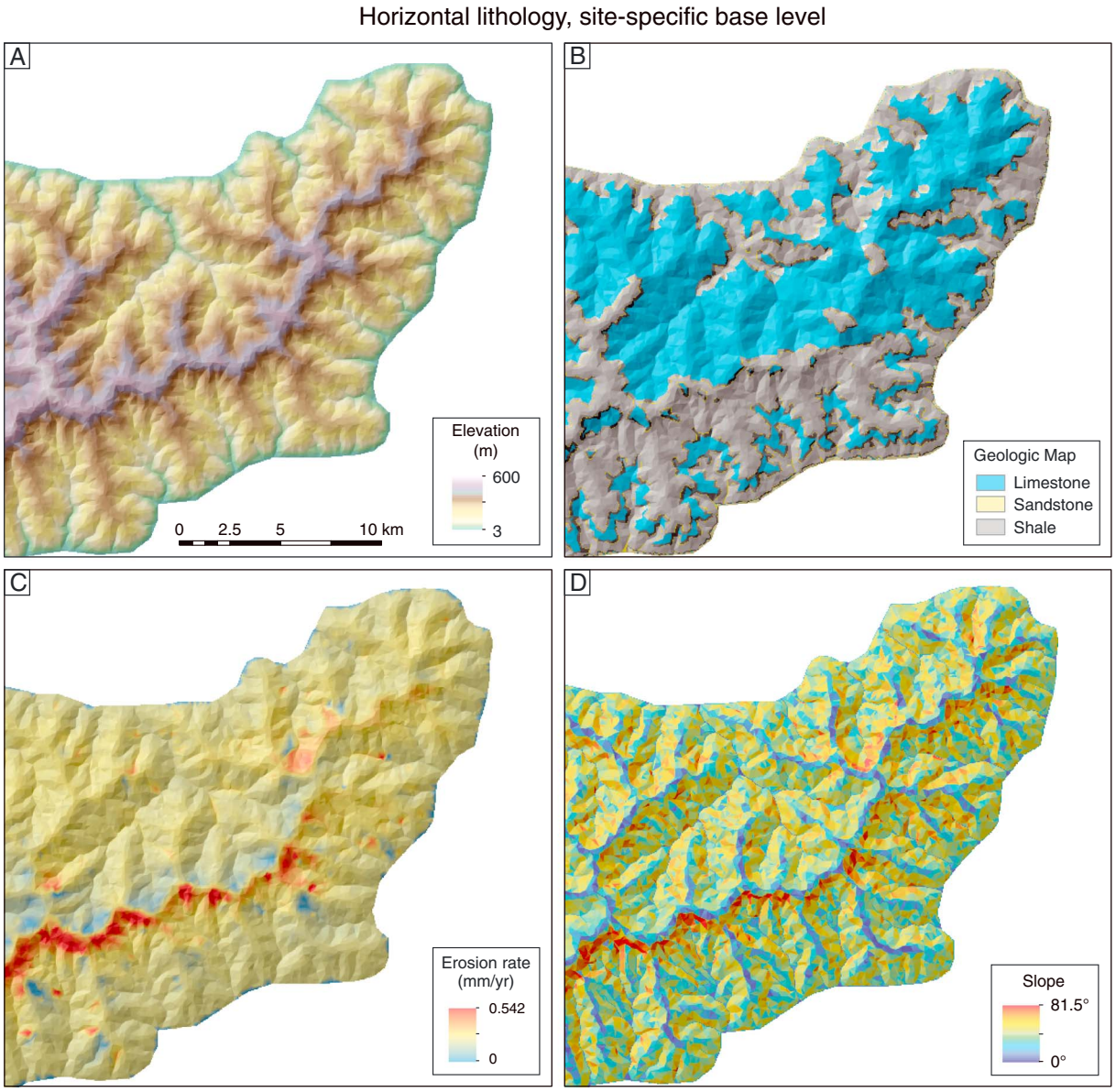

Figure 13. Topography of the best fit horizontal lithology simulation (HL047) at 10 Ma. (a) Modeled topography. (b) Erodibility map used in the simulation, which is for three rock types (limestone, sandstone, and shale) used in these simulations. Note the thin layer of sandstone beginning to be exhumed in the south (along the Aare River). (c) The spatial distribution of modeled erosion rates in the study area and (d) the distribution of modeled slopes.

4.3.1. Uniform and Steady Lithology Simulations

Erosion histories of the uniform lithology simulations follow the base level history changes of the landscape. During the early development of the landscape, erosion rates gradually increase toward the rate of rock uplift. This is most apparent in the results from the uniform rock uplift simulations (Figure 15a), where erosion rates increase monotonically with a delay that depends on the distance upstream from the base level change (denoted by the different colored lines in Figure 15). Close to the base level change (e.g., green lines), steady state erosion rates are reached in under 1 Ma. Midway up the catchment (blue lines), steady state is reached in ~16 Ma, and farther upstream, near the divide (red line) steady state is reached after 20 Ma of model simulation. This general effect of regions farthest from base level having a delayed response to the increase in erosion because of base level changes on the Rhine is applicable to all rivers in the eastern Jura Mountains.

In the tectonic and incision model where spatial and temporal variations in rock uplift and river capture events and subsequent incision are incorporated, abrupt changes in base level from either the start of

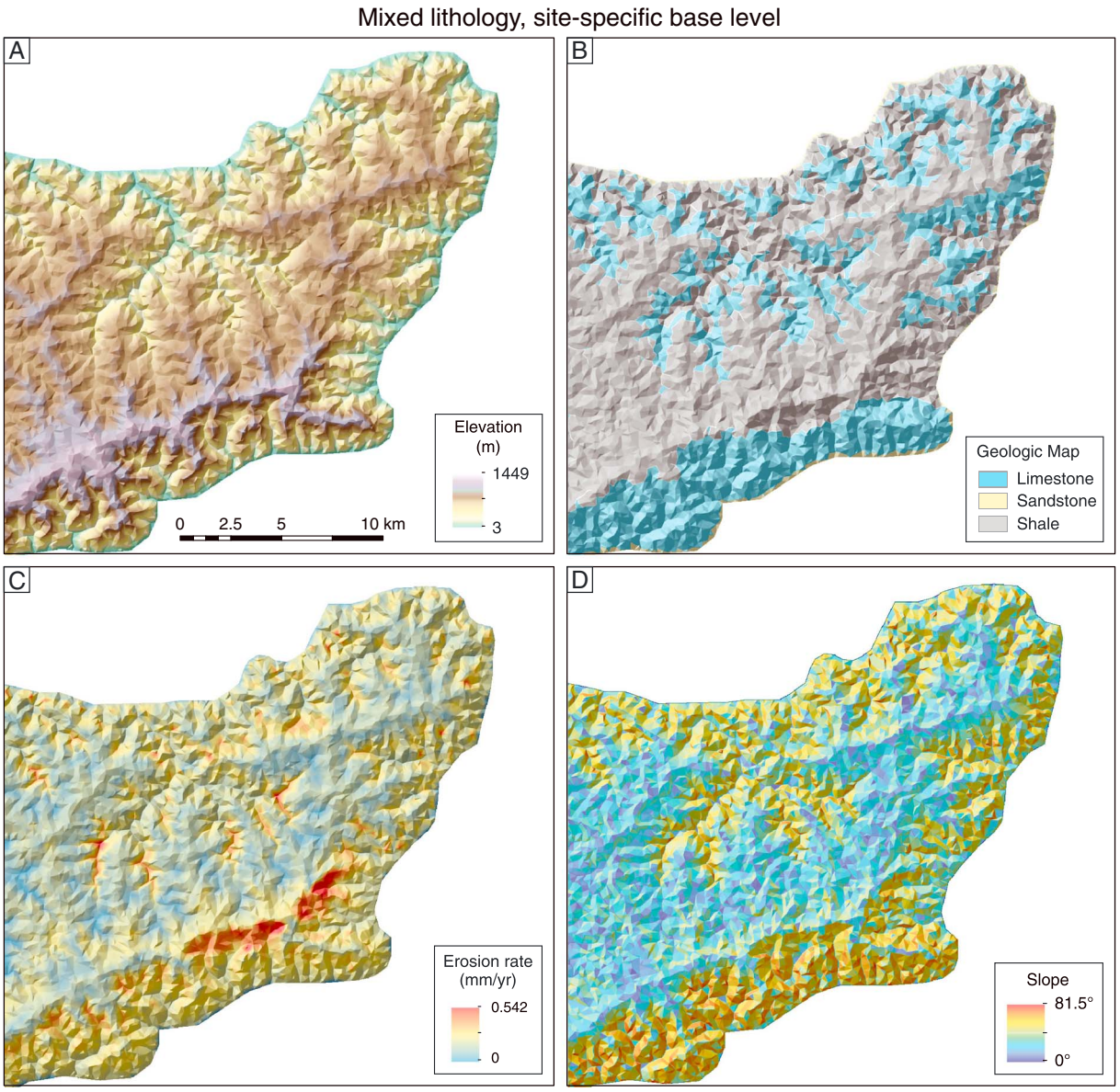

Figure 14. Map view of the mixed lithology (Figure 6d) case with site-specific rock uplift. (a) Modeled topography. (b) Erodibility map used in the simulation, which is just three rock types for these simulations. Note the thin layer of sandstone beginning to be exhumed in the south (along the Aare River). (c) The spatial distribution of modeled erosion rates in the study area and (d) the distribution of modeled landscape slopes.

deformation along a structure or incision due to drainage capture cause rapid increases in the erosion rate (Figure 15b). After the incision pulse passes or the structure becomes dormant, erosion rates decrease until they match the background rate of rock uplift. If the erosion rates are less than the background rate of rock uplift, however, they continue to increase until they reach the rate of rock uplift. The highest magnitude change in the erosion rate in response to a base level signal occurs near the model boundary (green line, Figure 15b); however, these high-magnitude pulses of erosion are short lived ($<$0.5 Ma). Farther upstream (blue and red lines, Figure 15b), the pulse of erosion is subdued (by an order of magnitude) but persists for a much longer time period (4–5 Ma after the capture event).

4.3.2. Nonuniform but Steady Lithology Simulations (Vertical Contacts)

In the uniform tectonic uplift model (Figure 15c), the nonuniform lithologies with temporally stable (vertical) lithology contacts also show a monotonic increase in erosion rate as the system approaches steady state similar to the uniform lithology case (compare previous section). However, there are a few important distinctions

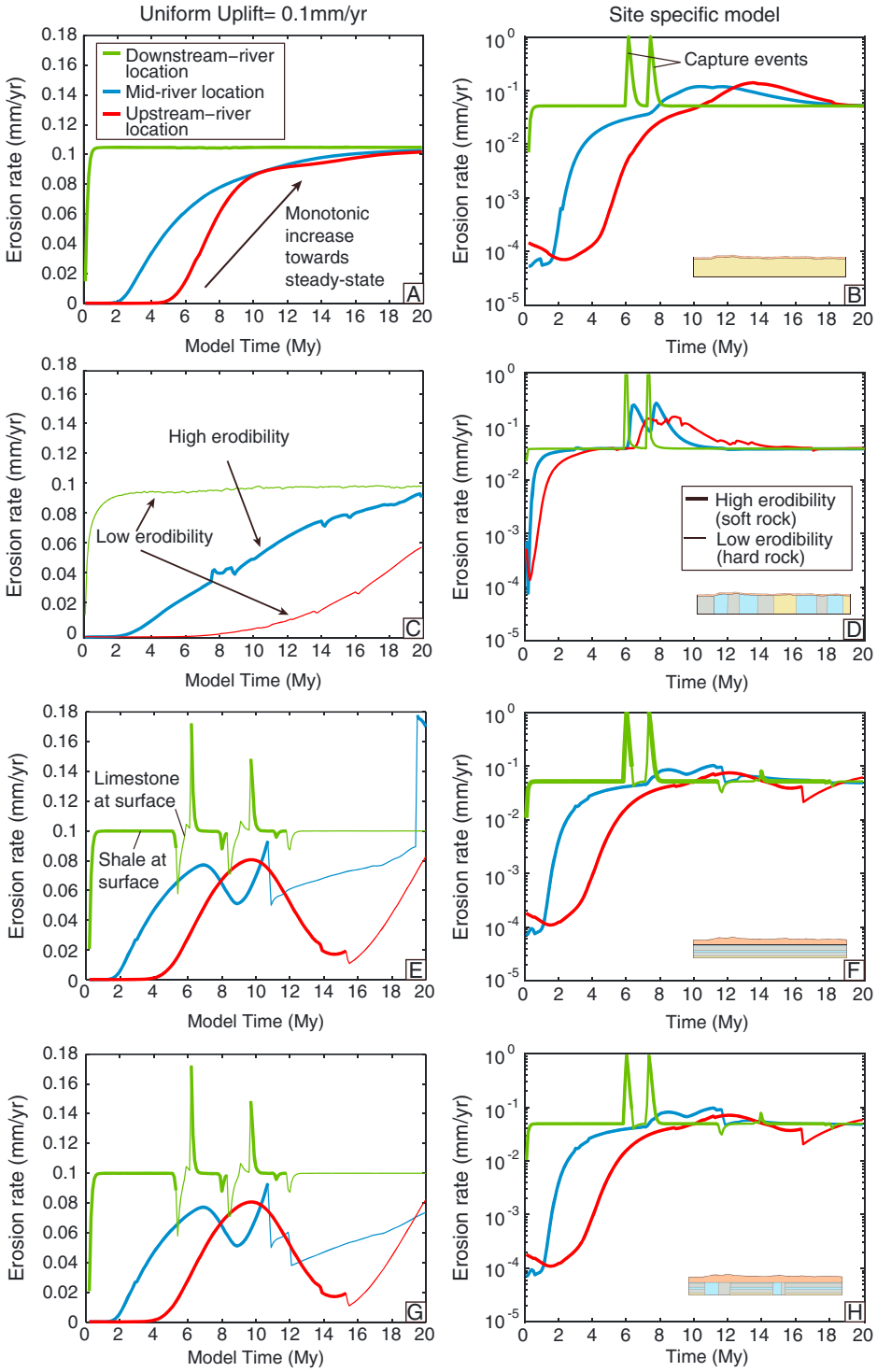

Figure 15. Erosion rate histories for different lithology and base level configurations. The lithology configuration is denoted by the inset diagram in Figures 15b, 15d, 15f, and 15h. The green lines correspond to the downstream location indicated in Figure 8, blue refers to the midstream position, and red refers to a position near the drainage divide. The lines are thick when shale is the surface lithology and thin when limestone is at the surface. (a, b) Uniform lithology, (c, d) vertical lithologic contacts, (e, f) horizontal lithology, and (g, h) the mix of horizontal and vertical lithologic contacts. Figures 15a, 15c, 15e, and 15g refer to the uniform uplift scenario, and Figures 15b, 15d, 15f, and 15h show the site-specific base level scenario inspired by the Neogene history of the Jura Mountains. Note the linear versus log scale of the *y* axis in the left and right columns. It should be also noted that much of the erosion rate variability in the uniform uplift cases (Figures 15a, 15c, 15e, and 15g) would be limited to 1 order of magnitude if a log scale were used.

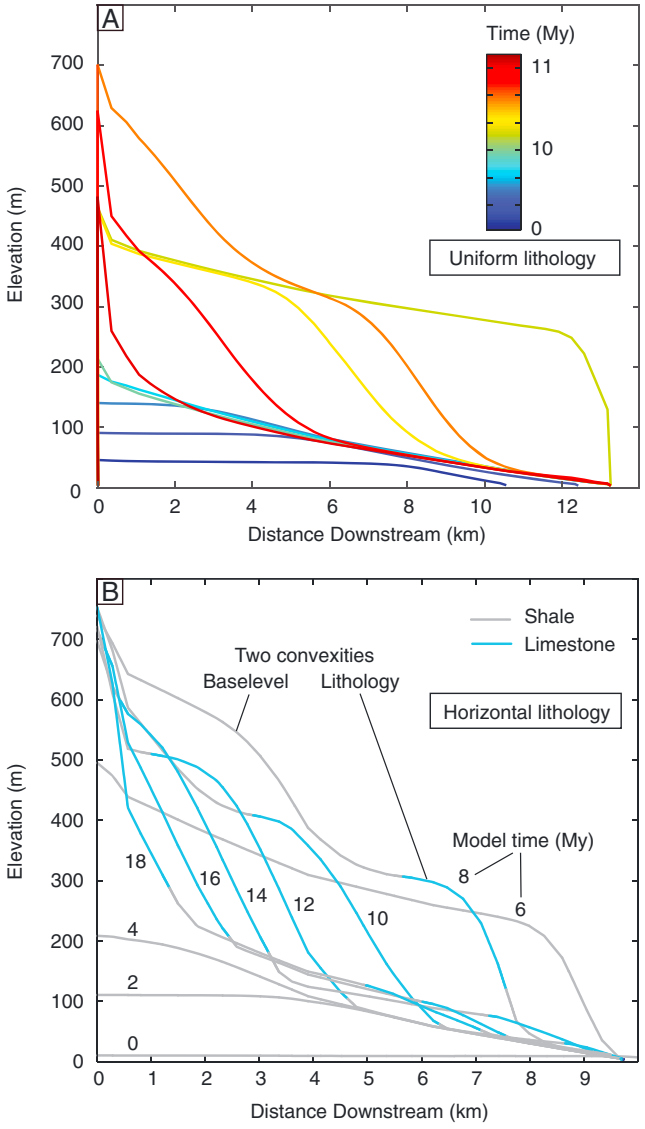

Figure 16. River profile evolution for the (a) uniform and (b) horizontal stratigraphy geometries considering the site-specific tectonic and base level scenario including capture events. The river profile location shown is from roughly the location of the red to green star in Figure 8a. The headwater location can fluctuate given the different lithologic conditions that lead to divide migration.

that result from the steady distribution of variable erodibility (Figure 15c). For example, near the model edge, the time to steady state is longer (green line, Figure 15C) compared to the uniform lithology case (green line, Figure 15a) due to the hard limestone of underlying bedrock. Because of the delay at the model edge, all locations upstream are delayed in achieving steady state as well even if they are located in the softer shale (e.g., midstream location, blue line in Figure 15c). The upstream location is in the hard limestone, and therefore, the delay to steady state is exacerbated.

In the site-specific base level model (i.e., spatially and temporally variable base level/rock uplift), the erosion pattern develops similar to the uniform lithology experiment yet with some important differences (Figure 15d). For example, two distinct pulses of erosion resulting from incision due to drainage capture are propagated to the midriver location (blue line, Figure 13b), whereas in the uniform lithology case, these pulses diffused into a broader wave of incision (compare Figures 15b and 15d). We note that the diffusion of the knickzone in a single lithology is a result of the choice of shear stress to approximate erosion (equation (1)) (Whipple & Tucker, 1999); however, when multiple rock types are present, transient waves (i.e., kinematic waves) will travel at different rates through the different erodibilities. Depending on the pattern of lithology through the drainage basin, this can accentuate or limit the magnitude of the diffusion of the base level signal. The similarities in the erosion history next to the model boundary, however, show that for the locations near the model boundary, the base level history dictates the maximum erosion rates, regardless of the rock type.

4.3.3. Nonuniform, Nonsteady Lithology Simulations (Horizontal and Mixed Lithology)

Under uniform uplift (Figure 15e) horizontally layered stratigraphy causes complicated erosion rate histories in different parts of the modeled landscape. For example, near the base level, the landscape quickly reaches steady state in the uppermost lithologic unit (Figure 15e). When the hard layer beneath is exposed, erosion rates lower as slopes increase to compensate for this harder rock type. Eventually, the softer shale beneath the limestone is exposed, increasing the rate of erosion (due to relatively steep slopes). Therefore, near the base level, the landscape responds with rapid and clear responses to changes in rock type. These signals of landscape transience (both the slowing of erosion and subsequent pulses) propagate upstream through the rest of the drainage basin and generate complex responses for the parts of the landscape not immediately next to the base level (Forte et al., 2016). This is because upstream from the base level, the landscape is sensitive to both local changes in erodibility and the previous downstream erosion responses to changes in erodibility (Figure 16). In other words, the response of downstream locations to changes in erodibility act as a change in relative base level for the river reaches upstream. For example, the midstream location analyzed in Figure 15e (blue line) responds to both downstream changes in erosion rates (e.g., the first dip in erosion at ~7 Ma) and changes in erosion due to the exposure of different rock types locally (e.g., the sharp changes in erosion rate when local lithology changes at ~10 Ma).

When applying the local tectonic and incision model, the erosion responses are overprinted with the spatial and temporal variations in rock uplift and the incisional waves due to drainage capture (Figure 15f). The incision waves that result because of the capture events lead to an order of magnitude greater increase in erosion rates than what is expected from just lithologic changes alone (note the *y* axis change in Figure 15f versus Figure 15b). However, this pulse of erosion is diffused farther upstream (blue line, Figure 15f),

meaning that the maximum magnitude lowers but the pulse of erosion persists for a longer period of time as the signal propagates upstream. The erosion pulse is essentially undetectable near the drainage divide (redline in Figure 15f). We note, however, that the base level signal does reach the drainage divide, but as the transience propagates through the different rock types in the landscape, the increase in erosion is spread out over greater time and lower magnitudes (maximum value of 0.075 mm/yr compared to the vertical contacts case which had a maximum value of 0.18 mm/yr). Thus, the integral of the signal remains the same (i.e., the total base level fall), but the timescale over which it occurs lengthens and thus the magnitude decreases.

Erosion histories of the mixed (horizontal and vertical) lithology cases for both uniform and tectonic scenarios are similar to the horizontal lithology histories outlined above. Minor differences such as a subdued erosion rate for the midriver location (blue line, Figure 15g) occur because of a second drop in erosion rate shortly after the exposure of the hard limestone layer. Further, minor differences occur at ~13 Ma of model simulations, but the very close erosion histories suggest that at our erosion history locations, chosen to provide a broad context across the landscape, are primarily driven by the horizontal lithology structure of the landscape. This is consistent with the results of Forte et al. (2016) who found that lithology had the greatest impact on landscape evolution when the dip of the contacts was low. We chose river locations that flow through a region with vertical contacts, but we note that the extent of zones with vertical contact is small compared to the model domain. Therefore, we conclude that if significant areas are underlain by horizontally bedded stratigraphy, the dynamics of those regions will strongly dictate the erosion history of the upstream landscape.

The evolution of modeled river profiles can help illuminate some of these complexities (Figure 16). Notice that multiple convexities can be seen at various times in the evolution of the river system, showing both lithologic and base level impacts on the development of the landscape (Figure 16). The rate at which these convexities transit upstream through the drainage system is dependent on the lithology, such that higher values of erodibility transmit the signal to upstream reaches faster. Therefore, the distance between two convexities can either increase when the higher erodibility is upstream (as in the highlighted case in Figure 16b) or decrease, with the potential for positive interference, when the higher erodibility is downstream. This adds a level of complexity to interpreting erosion rates and topographic transience in landscapes subject to both nonsteady base level and variable lithology.

5. Discussion

The results of this modeling study show that the erosion rate history at any given location depends on (1) the rock uplift and base level history, (2) the range of erodibility in the local stratigraphy, and (3) the history of surface geology along the entire river profile downstream of the location at which the erosion history is observed. This third factor is the reason for the increasingly complex erosion histories farther upstream. It is important to note that the effects of lithology on erosion rates depend on the contrast in erodibilities (e.g., difference between minimum and maximum values); therefore, estimating this range is important to understand the controls on landscape evolution in any region with heterogeneous lithology. In the following we discuss the above three points in more detail.

5.1. Rock Uplift and Base Level History

As illustrated by the erosion rate histories (Figure 15), changes of rock uplift/base level have a strong influence on landscape evolution, especially near the edge of the model boundary representing the local base level. For example, in nearly all cases, the biggest changes in erosion rates occur just after the capture events, which were responsible for a rapid base level fall of hundreds of meters (Figures 15b, 15d, 15f, and 15h). Moving away from the location of base level change, however, the signals are smeared out, which can happen due to complexities in lithologic structure (Forte et al., 2016) and model parameterization, such as the exponent on channel slope (Whipple & Tucker, 1999). The nature of the base level propagation has the effect to lower the absolute magnitude of erosion, but the integral of material removed must be the same; therefore, as the erosion rate magnitude decreases, the timescale of the response increases. This can be seen in Figure 15d where the midriver location has a lower maximum erosion rate, but the erosion pulse occurs over a longer time.

We use the context of the eastern Jura Mountains to show that the erosion rate history at any given location depends on the development of the surface geology along the entire river profile downstream of that location. This has important implications for considering erosion and exhumation rate histories in regions with complex lithology. Specifically, studies that consider the cause of changes in exhumation rates from techniques such as thermochronology must consider how lithologic variations may mimic or disrupt transient signals due to changes in rock uplift. Moreover, integral profile methods that require assumptions about the downstream distribution of erodibility (Perron & Royden, 2013) would require consideration of the temporal changes in downstream erodibility patterns in lithologically complex terrain (Whipple et al., 2017).

5.2. Range of Erodibility in the Local Stratigraphy

Numerical modeling offers an opportunity to quantify the relative importance of base level versus erodibility variations in landscapes subject to variable forcing. Observations of topography alone are insufficient to distinguish between base level versus lithologic causes of topographic variability. This is because in places where these factors vary over space and time, the landscape is in a constant state of transience. Our approach of using numerical modeling circumvents this problem by allowing for transience in the analysis (i.e., steady state is not a required assumption).

Previous estimates of tensile strength in a range of rock types ranged over 2 orders of magnitude, of which limestone and sandstone are near opposite ends of the spectrum (Sklar & Dietrich, 2001). These authors suggest that erosion scales with tensile strength squared, which would suggest a very large difference in erodibility for the lithologies considered in this study. However, we find that a twofold difference in erodibility between limestone and shale provides a reasonable fit to the topographic metrics considered here. This twofold difference is a much smaller range than predicted by the work of Sklar and Dietrich (2001). Therefore, it appears that complexities other than the susceptibility to abrasion (e.g., fracture spacing) influence the erosional resistance of a particular lithology within a stream power model context. A factor not captured by our approach is the different susceptibility to dissolution between limestone and the other rocks in the region. In certain environments, the dissolution of limestone can have a significant impact on mass removal from a river system (Covington, Gulley, & Gabrovšek, 2015). If dissolution is significant, a lower rate of physical erosion is necessary to remove mass in any equilibrium river profile setting. Because our modeling does not include dissolution, this may explain why erodibility values are closer than one would predict with tensile strength.

The manner in which a propagating base level signal is shredded by lithologically complex terrain depends on both the magnitude of base level change and the relative differences in erodibility. For example, if the slope change driven by a base level change far exceeds changes due to exposure of a different rock type, then the transient base level signal will propagate through the landscape with little impact due to changes in rock type. However, if the necessary slope change to accommodate the transient base level signal is similar to slope changes required to accommodate a different rock type, then we can expect the base level signal to be significantly impacted by complex lithology (Figure 16).

5.3. History of Surface Geology

Lithology plays a fundamental role in dictating how the propagation of the base level signals occurs. For example, compare Figures 15b, 15d, 15f, and 15h, illustrating erosion rates for models of different lithologic geometries but the same incision events. The influence on the erosion rates for the middle (blue line) and upper (red line) stream locations are distinctly different. For the vertical geology case (Figure 15d), the peaks at midstream are much more distinct than in the horizontal (Figure 15f) or mixed geology cases (Figure 15h). For the upstream location (red line), the pulses of stream capture are apparent in the vertical geology case, but in the horizontal and mixed geology cases, the base level signals diffuse and show only one coherent, long-lived pulse of erosion, peaking at around 12 Ma after the beginning of the simulation (~6 Ma after the first capture event).

Although the mixed lithology model produced somewhat more satisfactory topographic complexity than the horizontal simulations, the erosion rate histories were quite similar. This highlights an important result of this modeling: variations in erosion rate histories are strongly influenced by the broad representation of the regional geology (e.g., orientation of different lithologic units), whereas the complexity of topography is mainly controlled by local variation in erodibility. Thus, pulses of incision in lithologically complex terrains do not necessarily reflect changes of the base level (Forte et al., 2016). The exposure of different lithological units

can cause a significant transient landscape response to the change in erodibility at the surface (e.g., Figure 15e). Although the base level history is complicated, evidence from the uniform, steady uplift case provides information on how much of a change in the erosion rate can be expected if geomorphic processes eroded through one rock type and into another. For example, based on the modeling, we can expect up to an approximately twofold to threefold increase in erosion rates when rivers have completely incised through the hard limestone layers. This is evident at the midstream location (blue line, Figure 15e), for which the erosion rates increase from 0.09 mm/yr to ~0.18 mm/yr when the soft shale is exposed beneath the hard limestone at ~19 Ma.

6. Conclusion

A numerical landscape evolution model parameterized in the context of the geology and geomorphology of the eastern Jura Mountains was used to investigate general lithologic controls on landscape evolution. The first step of the analysis involved model calibration, in which it was found that using a twofold variation in erodibility between the hard limestone and soft shale best reflected the variability observed in modern topography. Following calibration, erosion histories for different parts of the model domain were quantified to explore increasingly complex scenarios of lithologic geometries. Additionally, both a uniform uplift model and a base level model inspired by the history of the eastern Jura Mountains were considered in order to evaluate how the lithological characteristics modulate the spatial and temporal landscape response to base level variation.

Our modeling work shows that differences in erodibility of lithologies play a fundamental role in landscape evolution by modulating the spatial and temporal response to landscape-shaping forces, in particular base level fall. The relative importance of base level fall versus lithological changes over space and time on local erosion history depends on the distance from base level and the differences in erodibility. Near the model boundary (here represented by rivers), the landscape responds rapidly and directly to the base level history. The rate at which pulses of erosion migrate through the landscape via the drainage system is dependent on the lithology such that the transient response is faster for higher values of erodibility. In general, the erosion history becomes more complicated upstream from the regional base level. This is because the effects of base level fall and lithologic changes become conflated, generating a complex erosion history, where distinguishing between the two effects becomes increasingly difficult. Specifically, lithologic knickpoints can continue to be "refreshed" as the contacts migrate through the landscape; however, once the base level-generated knickpoint migrates away from the model boundary, it becomes broader and wider due to the diffusion associated with choice of model parameters (Figure 16). A landscape is thus sensitive to both the local changes in erodibility and the downstream erosion histories. While the integral of the erosion pulse (i.e., the total base level fall) remains the same, the magnitude of the erosion rate decreases due to lengthening of the timescale over which it occurs.

Landscape history of a particular location is sensitive to both the local driving/resistance factors (i.e., local uplift/lithology) and the downstream landscape history. The latter is influenced by both base level evolution and lithologic changes. Studies focusing on the controls of landscape evolution should consider both the local changes in rock type and the evolution of rock type in the river system downstream of any local point of interest.

Acknowledgments

This study was supported in part by a contract from NAGRA (Swiss National Cooperative for the Disposal of Radioactive Waste) to T. A. E. A portion of this work was sponsored by the Army Research Laboratory and was accomplished under grant W911NF-15-1-0380 to B. J. Y. The views and conclusions contained in this document are those of the authors and should not be interpreted as representing the official policies, either expressed or implied, of the Army Research Laboratory or the U.S. Government. The U.S. Government is authorized to reproduce and distribute reprints for Government purposes notwithstanding any copyright notation herein. We thank Peter van der Beek, Amanda Keen-Zebert, an anonymous reviewer, and Associate Editor Mikael Attal for their thoughtful reviews that greatly improved this manuscript. The model codes and results will be stored in perpetuity at Indiana University's Scholarly Data Archive and are available by request to the author.

References

Becker, A. (2000). The Jura Mountains—An active foreland fold-and-thrust belt? *Tectonophysics*, *321*(4), 381–406. https://doi.org/10.1016/S0040-1951(00)00089-5

Bishop, P., & Goldrick, G. (2000). Geomorphological evolution of the east Australian continental margin. In M. A. Summerfield (Ed.), *Geomorphology and Global Tectonics* (pp. 227–255). Chichester, UK: Wiley.

Bishop, P., & Goldrick, G. (2010). Lithology and the evolution of bedrock rivers in post-orogenic settings: Constraints from the high-elevation passive continental margin of SE Australia. *Geological Society of London, Special Publication*, *346*(1), 267–287. https://doi.org/10.1144/SP346.14

Bishop, P., Young, R. W., & McDougall, I. (1985). Stream profile change and longterm landscape evolution: Early Miocene and modern rivers of the east Australian highland crest, central New South Wales, Australia. *Journal of Geology*, *93*(4), 455–474. https://doi.org/10.1086/628966

Brocard, G. Y., & van der Beek, P. A. (2006). Influence of incision rate, rock strength, and bedload supply on bedrock river gradients and valley-flat widths: Field-based evidence and calibrations from western alpine rivers (southeast France). *Geological Society of America Special Papers*, *398*, 101–126. https://doi.org/10.1130/2006.2398(07)

Burkhard, M. (1990). Aspects of the large-scale Miocene deformation in the most external part of the Swiss Alps (sub-Alpine molasse to Jura fold belt). *Eclogae Geologicae Helvetiae*, *83*(3), 559–583.

Burkhard, M., & Sommaruga, A. (1998). Evolution of the western Swiss Molasse basin: Structural relations with the Alps and the Jura belt. *Geological Society of London, Special Publication*, *134*(1), 279–298. https://doi.org/10.1144/GSL.SP.1998.134.01.13

Bursztyn, N., Pederson, J. L., Tressler, C., Mackley, R. D., & Mitchell, K. J. (2015). Rock strength along a fluvial transect of the Colorado Plateau—Quantifying a fundamental control on geomorphology. *Earth and Planetary Science Letters*, *429*, 90–100. https://doi.org/10.1016/j.epsl.2015.07.042

Champel, B., van der Beek, P., Mugnier, J.-L., & Leturmy, P. (2002). Growth and lateral propagation of fault-related folds in the Siwaliks of western Nepal: Rates, mechanisms, and geomorphic signature. *Journal of Geophysical Research*, *107*(B6), ETG 2-1. https://doi.org/10.1029/2001JB000578

Covington, M. D., Gulley, J. D., & Gabrovšek, F. (2015). Natural variations in calcite dissolution rates in streams: Controls, implications, and open questions. *Geophysical Research Letters*, *42*(8), 2,836–2,843. https://doi.org/10.1002/2015GL063044

Diebold, P., & Noack, T. (1997). Late Palaeozoic troughs and Tertiary structures in the eastern folded Jura. In O. A. Pfiffner, et al. (Eds.), *Deep Structure of the Swiss Alps* (pp. 59–63). Basel, CH: Birkhäuser.

Diebold, P., Bitterli-Brunner, P., & Naef, H. (2005). Geologischer Atlas der Schweiz 1:25′000, Blätter 1069/1049 Frick-Laufenburg, mit Erläuterungen. Wabern, CH: Bundesamt für Landestopographie swisstopo.

Forte, A. M., Yanites, B. J., & Whipple, K. X. (2016). Complexities of landscape evolution during incision through layered stratigraphy with contrasts in rock strength. *Earth Surface Processes and Landforms*, *41*(12), 1736–1757. https://doi.org/10.1002/esp.3947

Giamboni, M., Wetzel, A., Nivière, B., & Schumacher, M. (2004). Plio-Pleistocene folding in the southern Rhinegraben recorded by the evolution of the drainage network (Sundgau area; northwestern Switzerland and France). *Eclogae Geologicae Helvetiae*, *97*(1), 17–31. https://doi.org/10.1007/s00015-004-1112-4

Gilbert, G. K. (1877). *Report on the geology of the Henry Mountains*, Dept. of the Interior, U.S. Geographical and Geological Survey of the Rocky Mountain Region.

Goudie, A. S. (2016). Quantification of rock control in geomorphology. *Earth Science Reviews*, *159*, 374–387. https://doi.org/10.1016/j.earscirev.2016.06.012

Graf, H. R., Bitterli-Dreher, P., Burger, H., Bitterli, T., Diebold, P., & Naef, H. (2006). Geologischer Atlas der Schweiz 1:25′000, Blatt 1070 Baden, mit Erläuterungen. Wabern, CH: Bundesamt für Landestopographie swisstopo.

Herman, F., Seward, D., Valla, P. G., Carter, A., Kohn, B., Willett, S. D., & Ehlers, T. A. (2013). Worldwide acceleration of mountain erosion under a cooling climate. *Nature*, *504*(7480), 423–426. https://doi.org/10.1038/nature12877

Howard, A. D., & Kerby, G. (1983). Channel changes in badlands. *Geological Society of America Bulletin*, *94*(6), 739–752. https://doi.org/10.1130/0016-7606(1983)94%3C739:CCIB%3E2.0.CO;2

Isler, A., Pasquier, F., & Huber, M. (1984). Geologische Karte der zentralen Nordschweiz 1:100 000 mit angrenzenden Gebieten von Baden-Württemberg. *Geologische Spezialkarte 121*. Wabern, CH: Bundesamt für Landestopographie swisstopo.

Jansen, J. D., Codilean, A. T., Bishop, P., & Hoey, T. B. (2010). Scale dependence of lithological control on topography: Bedrock channel geometry and catchment morphometry in western Scotland. *Journal of Geology*, *118*(3), 223–246. https://doi.org/10.1086/651273

Jeffery, M. L., Ehlers, T. A., Yanites, B. J., & Poulsen, C. J. (2013). Quantifying the role of paleoclimate and Andean Plateau uplift on river incision. *Journal of Geophysical Research: Earth Surface*, *118*(2), 852–871. https://doi.org/10.1002/jgrf.20055

Jordan, P. (1992). Evidence for large-scale decoupling in the Triassic evaporites of northern Switzerland: An overview. *Eclogae Geologicae Helvetiae*, *85*(3), 677–693.

Jordan, P., Malz, A., Heuberger, S., Pietsch, J., Kley, J., & Madritsch, H. (2015). Regionale geologische Profilschnitte durch die Nordschweiz und 2D-Bilanzierung der Fernschubdeformation im östlichen Faltenjura: Arbeitsbericht zu SGT Etappe 2. *Nagra Arbeitsbericht NAB 14-105*. Wettingen, CH: Nagra.

Keen-Zebert, A., Tooth, S., & Stuart, F. M. (2016). Cosmogenic ^{3}He measurements provide insight into lithologic controls on bedrock channel incision: Examples from the South African Interior. *Journal of Geology*, *124*(3), 423–434. https://doi.org/10.1086/685506

Laubscher, H. P. (1972). Some overall aspects of Jura dynamics. *American Journal of Science*, *272*(4), 293–304. https://doi.org/10.2475/ajs.272.4.293

Lease, R. O., & Ehlers, T. A. (2013). Incision into the eastern Andean Plateau during Pliocene cooling. *Science*, *341*(6,147), 774–776. https://doi.org/10.1126/science.1239132

Madritsch, H. (2015). Outcrop-scale fracture systems in the Alpine foreland of central northern Switzerland: Kinematics and tectonic context. *Swiss Journal of Geosciences*, *108*(2-3), 155–181. https://doi.org/10.1007/s00015-015-0203-2

Madritsch, H., Fabbri, O., Hagedorn, E.-M., Preusser, F., Schmid, S. M., & Ziegler, P. A. (2010). Feedback between erosion and active deformation: Geomorphic constraints from the frontal Jura fold-and-thrust belt (eastern France). *International Journal of Earth Sciences*, *99*(S1), 103–122. https://doi.org/10.1007/s00531-009-0468-7

Malz, A., Madritsch, H., & Kley, J. (2015). Improving 2D seismic interpretation in challenging settings by integration of restoration techniques: A case study from the Jura fold-and-thrust belt (Switzerland). *Interpretation*, *3*(4), SAA37–SAA58. https://doi.org/10.1190/INT-2015-0012.1

Mazurek, M., Hurford, A. J., & Leu, W. (2006). Unravelling the multi-stage burial history of the Swiss Molasse Basin: Integration of apatite fission track, vitrinite reflectance and biomarker isomerisation analysis. *Basin Research*, *18*(1), 27–50. https://doi.org/10.1111/j.1365-2117.2006.00286.x

Miller, S. R., & Slingerland, R. L. (2006). Topographic advection on fault-bend folds: Inheritance of valley positions and the formation of wind gaps. *Geology*, *34*(9), 769–772. https://doi.org/10.1130/G22658.1

Pelletier, J. D., Engelder, T., Comeau, D., Hudson, A., Leclerc, M., Youberg, A., & Diniega, S. (2009). Tectonic and structural control of fluvial channel morphology in metamorphic core complexes: The example of the Catalina-Rincon core complex, Arizona. *Geosphere*, *5*(4), 363–384. https://doi.org/10.1130/GES00221.1

Perne, M., Covington, M. D., Thaler, E. A., & Myre, J. M. (2017). Steady state, erosional continuity, and the topography of landscapes developed in layered rocks. *Earth Surface Dynamics*, *5*(1), 85–100. https://doi.org/10.5194/esurf-5-85-2017

Perron, J. T., & Royden, L. (2013). An integral approach to bedrock river profile analysis. *Earth Surface Processes and Landforms*, *38*(6), 570–576. https://doi.org/10.1002/esp.3302

Petit, C., Campy, M., Chaline, J., & Bonvalot, J. (1996). Major palaeohydrographic changes in Alpine foreland during the Pliocene-Pleistocene. *Boreas*, *25*(2), 131–143.

Powell, J. W., Thompson, A. H., Coues, E., & Goode, G. B. (1875). *Exploration of the Colorado River of the West and Its Tributaries: Explored in 1869, 1870, 1871, and 1872, Under the Direction of the Secretary of the Smithsonian Institution*, U.S. government printing office.

Preusser, F., Graf, H. R., Keller, O., Krayss, E., & Schlüchter, C. (2011). Quaternary glaciation history of northern Switzerland. *EG Journal of Quaternary Science*, *60*, 282–305.

Rabin, M., Sue, C., Valla, P. G., Champagnac, J.-D., Carry, N., Bichet, V., … Mudry, J. (2015). Deciphering neotectonics from river profile analysis in the karst Jura Mountains (northern alpine foreland). *Swiss Journal of Geosciences*, *108*(2–3), 401–424. https://doi.org/10.1007/s00015-015-0200-5

Rahn, M. K., & Selbekk, R. (2007). Absolute dating of the youngest sediments of the Swiss Molasse basin by apatite fission track analysis. *Swiss Journal of Geosciences*, *100*(3), 371–381. https://doi.org/10.1007/s00015-007-1234-0

Roy, S. G., Tucker, G. E., Koons, P. O., Smith, S. M., & Upton, P. (2016). A fault runs through it: Modeling the influence of rock strength and grain-size distribution in a fault-damaged landscape. *Journal of Geophysical Research: Earth Surface*, *121*(10), 1911–1930. https://doi.org/10.1002/2015JF003662

Scharf, T. E., Codilean, A. T., de Wit, M., Jansen, J. D., & Kubik, P. W. (2013). Strong rocks sustain ancient postorogenic topography in southern Africa. *Geology*, *41*(3), 331–334. https://doi.org/10.1130/G33806.1

Schlunegger, F., & Mosar, J. (2010). The last erosional stage of the Molasse Basin and the Alps. *International Journal of Earth Sciences*, *100*(5), 1147–1162. https://doi.org/10.1007/s00531-010-0607-1

Sklar, L. S., & Dietrich, W. E. (2001). Sediment and rock strength controls on river incision into bedrock. *Geology*, *29*(12), 1,087–1,090. https://doi.org/10.1130/0091-7613(2001)029%3C1087:SARSCO%3E2.0.CO;2

Snyder, N. P., Whipple, K. X., Tucker, G. E., & Merritts, D. J. (2000). Landscape response to tectonic forcing: Digital elevation model analysis of stream profiles in the Mendocino triple junction region, northern California. *Geological Society of America Bulletin*, *112*(8), 1250–1263. https://doi.org/10.1130/0016-7606(2000)112%3C1250:LRTTFD%3E2.0.CO;2

Staškovanová, V., & Minár, J. (2016). Modelling the geomorphic history of the Tribeč Mts. and the Pohronský Inovec Mts. (Western Carpathians) with the CHILD model. *Open Geoscience*, *8*(1), 371–389. https://doi.org/10.1515/geo-2016-0038

Stock, J. D., & Montgomery, D. R. (1999). Geologic constraints on bedrock river incision using the stream power law. *Journal of Geophysical Research*, *104*(B3), 4983–4993. https://doi.org/10.1029/98JB02139

Tucker, G. E. (2004). Drainage basin sensitivity to tectonic and climatic forcing: Implications of a stochastic model for the role of entrainment and erosion thresholds. *Earth Surface Processes and Landforms*, *29*(2), 185–205. https://doi.org/10.1002/esp.1020

Tucker, G. E., & Slingerland, R. (1996). Predicting sediment flux from fold and thrust belts. *Basin Research*, *8*(3), 329–349. https://doi.org/10.1046/j.1365-2117.1996.00238.x

Tucker, G. E., & Slingerland, R. (1997). Drainage basin responses to climate change. *Water Resources Research*, *33*(8), 2031–2047. https://doi.org/10.1029/97WR00409

Tucker, G. E., Lancaster, S. T., Gasparini, N. M., Bras, R. L., & Rybarczyk, S. M. (2001). An object-oriented framework for distributed hydrologic and geomorphic modeling using triangulated irregular networks. *Computational Geosciences*, *27*(8), 959–973. https://doi.org/16/S0098-3004(00)00134-5

van der Beek, P., Pulford, A., & Braun, J. (2001). Cenozoic landscape development in the Blue Mountains (SE Australia): Lithological and tectonic controls on rifted margin. *Journal of Geology*, *109*(1), 35–56. https://doi.org/10.1086/317963

Van Der Beek, P., & Braun, J. (1998). Numerical modelling of landscape evolution on geological time-scales: A parameter analysis and comparison with the south-eastern highlands of Australia. *Basin Research*, *10*(1), 49–68. https://doi.org/10.1046/j.1365-2117.1998.00056.x

von Hagke, C., Cederbom, C. E., Oncken, O., Stöckli, D. F., Rahn, M. K., & Schlunegger, F. (2012). Linking the northern Alps with their foreland: The latest exhumation history resolved by low-temperature thermochronology. *Tectonics*, *31*(5), TC5010. https://doi.org/10.1029/2011TC003078

Whipple, K. X. (2001). Fluvial landscape response time: How plausible is steady-state denudation? *American Journal of Science*, *301*(4-5), 313–325. https://doi.org/10.2475/ajs.301.4-5.313

Whipple, K. X., & Meade, B. J. (2006). Orogen response to changes in climatic and tectonic forcing. *Earth and Planetary Science Letters*, *243*(1–2), 218–228. https://doi.org/10.1016/j.epsl.2005.12.022

Whipple, K. X., & Tucker, G. E. (1999). Dynamics of the stream-power river incision model: Implications for height limits of mountain ranges, landscape response timescales, and research needs. *Journal of Geophysical Research*, *104*(B8), 17,661–17,674. https://doi.org/10.1029/1999JB900120

Whipple, K. X., & Tucker, G. E. (2002). Implications of sediment-flux-dependent river incision models for landscape evolution. *Journal of Geophysical Research*, *107*, 2039. https://doi.org/10.1029/2000JB000044

Whipple, K. X., Forte, A. M., DiBiase, R. A., Gasparini, N. M., & Ouimet, W. B. (2017). Timescales of landscape response to divide migration and drainage capture: Implications for the role of divide mobility in landscape evolution. *Journal of Geophysical Research: Earth Surface*, *122*, 248–273. https://doi.org/10.1002/2016JF003973

Whitbread, K., Jansen, J., Bishop, P., & Attal, M. (2015). Substrate, sediment, and slope controls on bedrock channel geometry in postglacial streams. *Journal of Geophysical Research: Earth Surface*, *120*, 779–798. https://doi.org/10.1002/2014JF003295

Willenbring, J. K., & von Blanckenburg, F. (2010). Long-term stability of global erosion rates and weathering during late-Cenozoic cooling. *Nature*, *465*(7295), 211–214. https://doi.org/10.1038/nature09044

Willett, S. D. (1999). Orogeny and orography: The effects of erosion on the structure of mountain belts. *Journal of Geophysical Research*, *104*(B12), 28,957–28,981. https://doi.org/10.1029/1999JB900248

Willett, S. D., & Schlunegger, F. (2010). The last phase of deposition in the Swiss Molasse Basin: From foredeep to negative-alpha basin. *Basin Research*, *22*(5), 623–639. https://doi.org/10.1111/j.1365-2117.2009.00435.x

Willett, S. D., McCoy, S. W., Perron, J. T., Goren, L., & Chen, C.-Y. (2014). Dynamic reorganization of river basins. *Science*, *343*(6175), 1248765. https://doi.org/10.1126/science.1248765

Wobus, C., Whipple, K. X., Kirby, E., Snyder, N., Johnson, J., Spyropolou, K., … Sheehan, D. (2006). Tectonics from topography: Procedures, promise, and pitfalls. *Geological Society of America Special Papers*, *398*, 55–74. https://doi.org/10.1130/2006.2398(04)

Yanites, B. J., & Kesler, S. E. (2015). A climate signal in exhumation patterns revealed by porphyry copper deposits. *Nature Geoscience*, *8*(6), 462–465. https://doi.org/10.1038/ngeo2429

Yanites, B. J., Ehlers, T. A., Becker, J. K., Schnellmann, M., & Heuberger, S. (2013). High magnitude and rapid incision from river capture: Rhine River, Switzerland. *Journal of Geophysical Research: Earth Surface*, *118*, 1060–1084. https://doi.org/10.1002/jgrf.20056

Ziegler, P. A., & Fraefel, M. (2009). Response of drainage systems to Neogene evolution of the Jura fold-thrust belt and Upper Rhine Graben. *Swiss Journal of Geosciences*, *102*(1), 57–75. https://doi.org/10.1007/s00015-009-1306-4